Tim Sumner
DPhil. U. of Sussex
1979: Progress towards a new expt. to search for the neutron EDM.

CHAPTER 2

MAGNETIC SHIELDING.

By way of an introduction to this section, a chronological account of the relevant contributions is probably the best way to obtain a feeling for the level of understanding existing in this field in the mid-1970's when this work was initiated. For the sake of completeness one should mention that the first publication concerning magnetic shielding was that of della Porta[18] in 1589. However, it required a further three centuries before Rucker[19] in 1894 produced a mathematical solution for the transverse static shielding of multi-layer concentric shields. He showed that a much greater shielding factor can be obtained by using two thin concentric layers separated by an air gap, rather than one layer with twice the thickness. A little later, in 1899, Wills[20] published his 'simplified' calculations for the transverse static shielding of concentric three-layer cylindrical and spherical magnetic shields. Since then there have been several publications[21-25] presenting simplifications and generalisations for these calculations. In 1912 Esmarch[26] performed a series of experiments to investigate the variation of the transverse static shielding factor with position along the axis of open-ended multi-layer cylindrical shields. He also studied the variation with the number of layers, up to a maximum of 63 layers. The next publication, 22 years later, by Schelkunoff[27] concerned shielding against alternating electromagnetic fields. There is then a further gap of 23 years before the discovery of any novel effects, when Albach & Voss[28] investigated a

method of enhancing the magnetic shielding against low frequency disturbances, by applying an alternating (shaking) magnetic field to the sheild. Then in 1968 Mager[29] produced the first discussion of the axial shielding properties for single layer cylindrical shields and two years later extended his results for two-layer systems[30]. Apart from some specific experiments which have used magnetic shields of necessity, (for example: the stable operation of hydrogen masers[31], shielded rooms[32-35], measurements of the electric[5] and magnetic[36] dipole moments of the neutron, and some optical pumping experiments at very low magnetic fields $\sim 10^{-13}$ T[37,38]) this appeared to be the 'state of the art' up to the mid-1970's.

The reason that so little progress seems to have been made is due to the fact that, until recently, the applications requiring shielding, (and here should be included cathode ray tube shields, photomultiplier tube shields, etc.) have needed a level of shielding which was easily and relatively cheaply obtainable. However with the inevitable advent of much more demanding experiments, in particlar the two in which this group at the University of Sussex is involved,[39] there is now a need for a deeper understanding of the problem. With the realization that the success or failure of the proposed EDM experiment would ultimately depend on the time stability of the magnetic field, (not to mention an estimated cost in excess of £10,000) it was decided that there was insufficent data available to allow an immediate design of a suitable shielding assembly. In particular the limited knowledge of the axial shielding properties of multi-layer cylindrical shields. Hence

a study of magnetic shielding and its problems was undertaken. About the same time a similar study was under way in the Soviet Union,[40-45] in preparation for their own EDM experiment.[46,47] In this chapter a general review of magnetic shielding is presented in an effort to remove certain misunderstandings which seem to be prevalent. The discussion is purposely restricted to conventional cylindrical magnetic shielding although a short section on superconducting shielding is included at the end. A recursion formula for the calculation of the transverse static shielding of multi-layer cylindrical shields is given, which is particularly amenable to numerical computation and has the added advantage of providing the shielding factors of each sub-assembly before the addition of the next outer layer. An alternative method for calculating the axial static shielding factors for multi-layer cylindrical shields is derived. Finally, an experimental study is reported, using a prototype four-layer mu-metal shield. The results from this prototype and from other shields, where data is available, are compared with theory, particularly with respect to the axial shielding performance, and a design for a full size assembly for the EDM experiment is evaluated. Although most of the theory is developed ignoring the ferromagnetic nature of the shielding material, there are certain aspects of the behaviour which do require some discussion of ferromagnetism. With this in mind, in the following section, some of the more relevant features of ferromagnetism are discussed before proceeding to the general topic of magnetic shielding.

2·1 Ferromagnetism.

It will be shown later that the shielding factor obtained for a single layer shield is proportional to its relative magnetic permeability, μ. However, in reality, μ is not only a highly non-linear function of the flux density, B_m, in the material but is also dependent on the exact magnetic history of the material. Bearing this in mind it is useful to consider two features of ferromagnetism.

(a) The normal magnetisation curve and its behaviour around $B_m = H_m = 0$, and,

(b) the response of the magnetic state of the material to cyclic variations in the external field.

These two features will now be dealt with in turn.

(a) The normal magnetisation curve.

The materials normally used for magnetic shields are those with the highest permeabilities, and most common amongst these are the permalloy and mu-metal groups. For the most part the discussion will be in terms of these materials. In FIG 2·1 are shown the complete hysteresis loops for (a) 4-79 permalloy, and (b) mu-metal. Curve (a) is redrawn from Bozorth[48 p480] while curve (b) is an experimental curve measured as in Appendix A. The portion OA of each curve (redrawn for the case of mu-metal in FIG 2·2) is called the normal magnetisation curve, and describes the variation of B_m and H_m when starting from the initial state $B_m = H_m = 0$. The form of this curve near the origin is found to be accurately described by the Rayleigh[49] relation:-

$$\mu\mu_o = \mu_1\mu_o + \nu H_m \qquad 2\cdot1$$

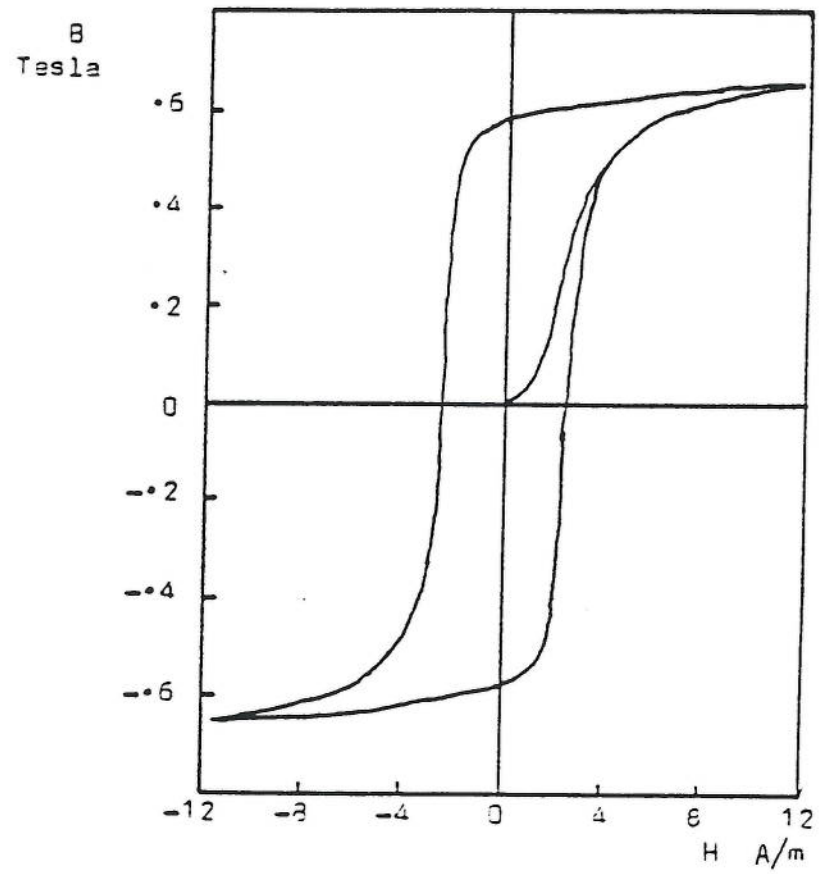

FIG 2•1(a) : B-H curve in 4-79 permalloy.

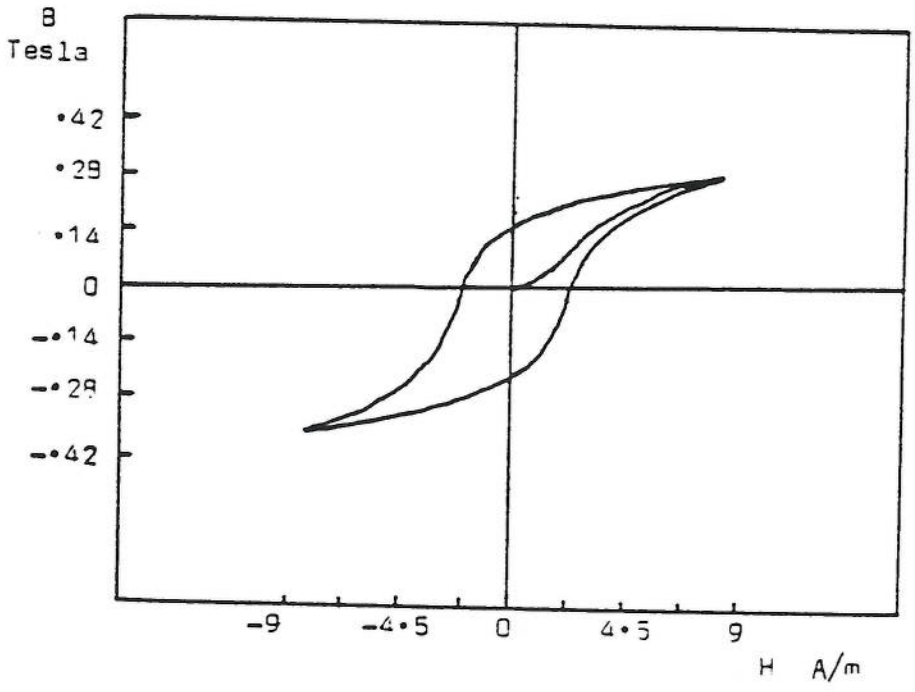

FIG 2•1(b) : B-H curve in mu-metal.

where μ_1 is the initial relative permeability (see FIG 2•2) and ν is some parameter dependent on the material.

Equation 2•1 can be rewritten in terms of the flux density, B_m, as:-

$$\mu = \tfrac{1}{2}(\mu_1 + (\mu_1^2 + \frac{4\nu B_m}{\mu_o})^{\frac{1}{2}}) \qquad 2•2$$

(b) Response to cyclic perturbations.

FIG 2•3 shows the response of a sample, originally in the state $B_m = B$, $H_m = H$, to a periodic variation in H_m of amplitude H_1. The response during the first cycle of the perturbation will depend on the direction of the initial variation with respect to H_m, as can be seen by comparing the response to the variations OAOBOA and OCOAOB in FIG 2•3. However after at least one cycle the magnetic state of the material will follow the minor loop AB. The slope of the line AB joining the extreme tips of the minor loop is a measure of the so called incremental permeability. For a given perturbation amplitude this slope is almost independent of the value of H_m, as can be seen in FIG 2•4(a). If on the other hand H_m is kept fixed and the perturbation amplitude varied the slope of the minor loops will change as in FIG 2•4(b). It is found that the slope of these loops is also described by the Rayleigh relation:-[49]

$$\mu = \tfrac{1}{2}(\mu_1 + (\mu_1^2 + \frac{4\nu \Delta B_m}{\mu_o})^{\frac{1}{2}}) \qquad 2•3$$

where ΔB_m is now the peak to peak variation in B_m.

Finally, before moving on to the shielding theory, it is worth

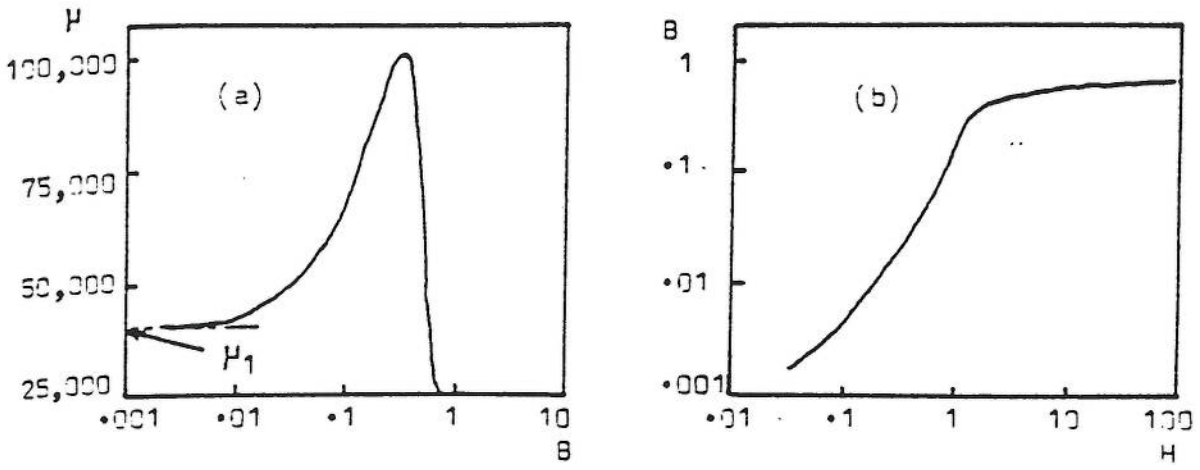

FIG 2·2 : Variation of permeability, μ, and magnetic field strength, H, with flux density, B, for mu-metal.

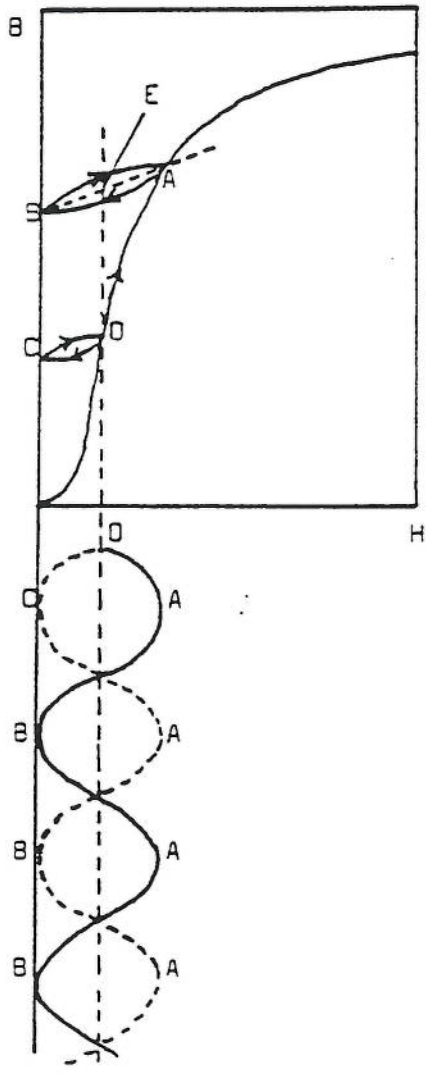

FIG 2·3 : Effect of a superposed a.c. perturbation.

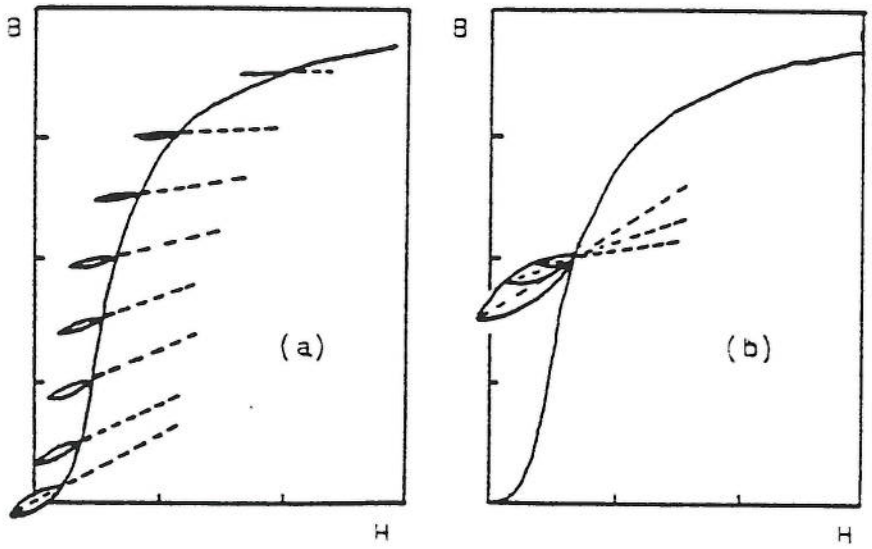

FIG 2•4 : Behaviour of minor hysteresis loops with (a) steady field, H_m, and, (b) the perturbation amplitude, H_1.

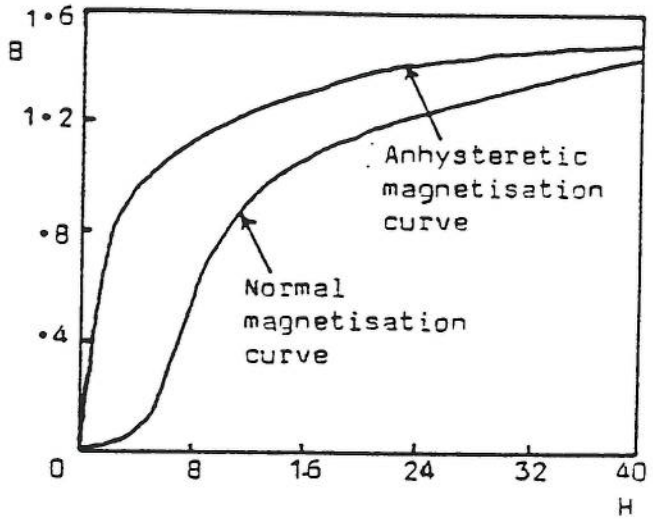

FIG 2•5 : Anhysteretic magnetisation curve (for iron).

examining what happens when a periodic perturbation is applied and then slowly reduced to zero. Returning to FIG 2•3, in that case the minor loop AB gradually collapses to leave the material in the state corresponding to point E. At point E the effective permeability, B_m/H_m, is much higher than at the original point O. If the initial amplitude of the perturbation is allowed to drive the material into saturation in both directions before it is reduced to zero the point E, as a function of H_m, will then describe the ideal or anhysteretic magnetisation curve. This curve follows the mid-points of the major hysteresis loop and is shown in FIG 2•5 for the case of iron.

2•2 Transverse magnetic shielding.

In practice the real problem of a finite closed cylinder in a uniform magnetic field, B_o, as shown in FIG 2•6, is never solved. Instead the solution for infinitely long cylinders is used as this situation is exactly soluble[20]. The assumption is usually made that the end-caps, to some extent, compensate for the reduced length. Pendlebury[50] has considered this problem using a method based on flux gathering and reluctance theory and concludes that for a single layer, with length to radius ratio > 1, deviations from this assumption are likely to be small. Hence in this section a further solution to the infinite cylinder situation will be presented which is particularly amenable to numerical computation.

Assuming the relative permeability, μ, to be constant throughout each region of the shielding material (see FIG 2•6(b)) the equation to be solved is Laplace's equation for the magnetic scalar potential, ϕ:-

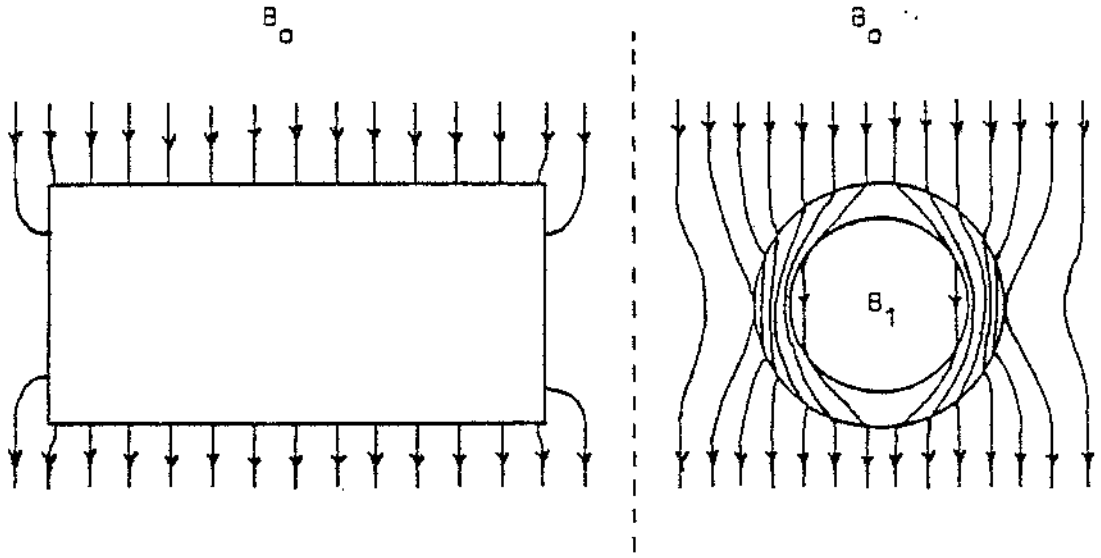

FIG 2·6(a) : Transverse shielding by a single finite cylinder.

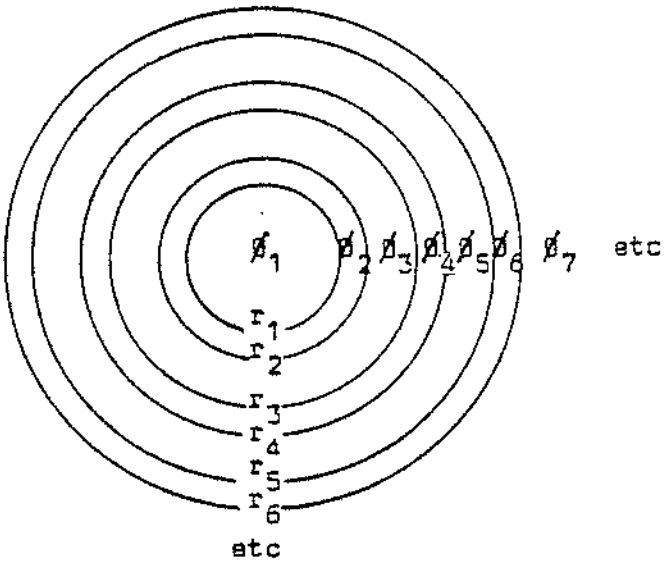

FIG 2·6(b) : Multiple-layer transverse shielding configuration.

$$\nabla^2 \phi = 0 \qquad 2\cdot4$$

where $$\underline{H} = -\nabla\underline{\phi} \qquad 2\cdot5$$

The following boundary conditions must be satisfied at all boundaries:-

(i) the normal component of $\underline{B}$ is continuous, and,

(ii) the tangential component of $\underline{H}$ is continuous.

Working in cylindrical polar coordinates (ρ,θ,z) the scalar potential in each region can be written:-

$$\phi_k = (C_k\rho + \frac{D_k}{\rho})\cos\theta \qquad 2\cdot6$$

and the two boundary conditions are:-

$$\mu_k \frac{d\phi}{d\rho}\Big|_{r_k} = \mu_{k+1}\frac{d\phi}{d\rho}_{k+1}\Big|_{r_k} \qquad 2\cdot7(a)$$

and $$\frac{1}{r_k}\frac{d\phi}{d\theta}_k\Big|_{r_k} = \frac{1}{r_k}\frac{d\phi}{d\theta}_{k+1}\Big|_{r_k} \qquad 2\cdot7(b)$$

where r_k is the radius of the k^{th} boundary (see FIG 2·6(b)). In the centre region, for ϕ_1 to remain finite $D_1 = 0$ and thus the magnetic field, B_1, in the centre region is:-

$$B_1 = -\mu_o C_1(\cos\theta.\hat{\underline{\rho}} - \sin\theta.\hat{\underline{\theta}}) \qquad 2\cdot8$$

which is a uniform field of magnitude $\mu_o C_1$.

For an n-layer shield the field outside, B_{2n+1}, will be:-

$$B_{2n+1} = -\mu_o(C_{2n+1} - \frac{D}{\rho^2}2n+1)\cos\theta.\hat{\underline{\rho}} + \mu_o(C_{2n+1} + \frac{D}{\rho^2}2n+1)\sin\theta.\hat{\underline{\theta}} \qquad 2\cdot9(a)$$

which for large distances becomes:-

$$B_o = -\mu_o C_{2n+1}(\cos\theta.\hat{\underline{\rho}} - \sin\theta.\hat{\underline{\theta}}) \qquad 2\cdot9(b)$$

which is again a uniform field, of magnitude $\mu_o C_{2n+1}$.
The shielding factor, S^T, is then defined as:-

$$S^T = \frac{B_o}{B_1} = \frac{C}{C_1}2n+1 \qquad 2\cdot10(a)$$

Putting C_1 arbitrarily to 1 this becomes:-

$$S^T = C_{2n+1} \qquad 2\cdot10(b)$$

The subscript 2n+1 is always odd and substituting 2·6 into 2·7 gives, for k odd:-

$$C_{k+1} = \tfrac{1}{2}(C_k(1 + \frac{1}{\mu_m}) + \frac{D_k}{r_k^2}(1 - \frac{1}{\mu_m})) \qquad 2\cdot11(a)$$

$$D_{k+1} = \tfrac{1}{2}(C_k r_k^2(1 - \frac{1}{\mu_m}) + D_k(1 + \frac{1}{\mu_m})) \qquad 2\cdot11(b)$$

where m = (k + 1)/2 and μ_m is the relative permeability of the m^{th}-layer of shielding material.

From 2·11 :-

$$C_{k+2} = \tfrac{1}{4}C_k\left(\left(2+\frac{1}{\mu_m}+\mu_m\right)+\left(\frac{r_k}{r_{k+1}}\right)^2\left(2-\frac{1}{\mu_m}-\mu_m\right)\right) + \tfrac{1}{4}D_k\left(\mu_m-\frac{1}{\mu_m}\right)\left(\frac{1}{r_k^2}-\frac{1}{r_{k+1}^2}\right) \qquad 2\cdot12(a)$$

$$D_{k+2} = \tfrac{1}{4}C_k\left(\mu_m-\frac{1}{\mu_m}\right)\left(r_k^2-r_{k+1}^2\right) + \tfrac{1}{4}D_k\left(\left(2+\frac{1}{\mu_m}+\mu_m\right)+\left(\frac{r_{k+1}}{r_k}\right)^2\left(2-\frac{1}{\mu_m}-\mu_m\right)\right) \qquad 2\cdot12(b)$$

These recursion relations can be greatlysimplified by making the following two assumptions:-

(i) $\mu_m \gg 1$, and,

(ii) $t \ll R_m$.

t is the shielding material thickness and R_m the average radius of the m^{th}-layer given by:-

$$R_m = r_k + \frac{t}{2} = r_{k+1} - \frac{t}{2} \qquad 2\cdot13$$

where k=2m+1 is always odd.

Substituting 2·13 into 2·12 and making the above assumptions yields:-

$$C_{k+2} = C_k\left(1 + \frac{\mu_m t}{2R_m}\right) + D_k\left(\frac{\mu_m t}{2R_m^3}\right) \qquad 2\cdot14(a)$$

$$D_{k+2} = -C_k\left(\frac{\mu_m}{2}tR_m\right) + D_k\left(1 - \frac{\mu_m t}{2R_m}\right) \qquad 2\cdot14(b)$$

For a single layer the shielding factor becomes:-

$$S_1^T = C_3 = 1 + \frac{\mu_1 t}{2R_1} \qquad 2\cdot15$$

In most cases $S_1^T \gg 1$ and the 1 can be ignored.

For a two-layer system equations 2·14 give:-

$$S^T = C_5 = (1 + \frac{\mu_2 t}{2R_2})C_3 + (\frac{\mu_2 t}{2R_2^3})D_3$$

$$= 1 + \frac{\mu_2 t}{2R_2} + \frac{\mu_1 t}{2R_1} + \frac{\mu_1 \mu_2 t^2}{4R_1 R_2}(1 - (\frac{R}{R_2}1)^2) \qquad 2\cdot16$$

This can be rewritten as:-

$$S^T \simeq S_1^T + S_2^T + S_1^T S_2^T(1 - (\frac{R}{R_2}1)^2) \qquad 2\cdot17$$

where $S_i^T = \frac{\mu_i t}{2R_i}$.

This result can be similarly generalised to n-layers:-

$$S^T = \sum_{i=0}^{n} S_i^T + \sum_{i,j}^{n-1,n} \sum_{i} S_i^T S_j^T (1 - (\frac{R_i}{R_j})^2)$$

$$+ \sum_{i,j}^{n-2,n-1,n} \sum_{i,k} \sum_{j} S_i^T S_j^T S_k^T (1 - (\frac{R_j}{R_k})^2)(1 - (\frac{R_i}{R_j})^2) \qquad 2\cdot18$$

$$+ S_1^T S_2^T \ldots S_n^T (1-(\frac{R}{R_2}1)^2)(1-(\frac{R}{R_3}2)^2)\ldots(1-(\frac{R}{R_n}-1)^2)$$

In general the last term is usually dominant, going as μ^n, in which case equation 2·18 can be approximated by:-

$$S^T = \prod_{i=1}^{n-1} S_n^T S_i^T (1 - (\frac{R_i}{R_{i+1}})^2) \qquad 2\cdot19$$

The presence of the factors $(1 - (\frac{R_i}{R_{i+1}})^2)$ demonstrates clearly the need for substantial air gaps between layers, first realised by Rucker[19]. However, as the layers become larger their

individual shielding factors are falling as $\frac{1}{r}$ and hence there is some optimum arrangement. This turns out[20,44] to be a geometric progression in the radii:-

$$R_{i+1} = \alpha R_i \qquad 2\cdot20$$

although the variation is rather slow. The next question to ask is whether, if the inner and outer radii are fixed, there is an optimum number of layers to use. In FIG 2·7(a) is shown a specific example of the variation of S^T with n for a shield with R_1 = 0·5m and R_n = 1·0m. 1mm material is used with a permeability of 30,000. Although the curve is beginning to flatten out there is no sign of a maximum up to n = 20. The dotted line would be the shielding obtained with a single solid layer. The same shielding factor can be achieved using only four 1mm thick layers suitably arranged, i.e. using only 1% of the material. In order to see a maximum curve (b) is plotted for R_1 = 0·5m and R_n = 0·53m. For n = 20 the first two layers are then touching. The maximum occurs for n = 14 when the average separation between layers is only 2·3 times the thickness. Hence, in practice, for such high permeability materials the maximum number of layers, between two given radii, will be determined by cost rather than by performance. Again the dotted line in curve (b) is for a single solid layer.

In view of the results in FIG 2·7 the original question can be reworded. Given n layers, with a fixed inner radius, what is the optimum value of α to use in equation 2·20 ? Results of calculations along these lines are shown in FIG 2·8 for the

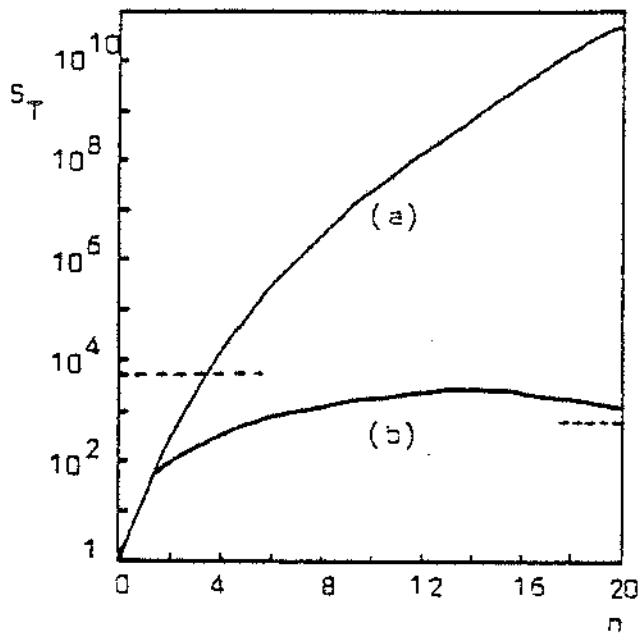

FIG 2·7 : Variation of shielding factor, S_T, with number of layers, n.

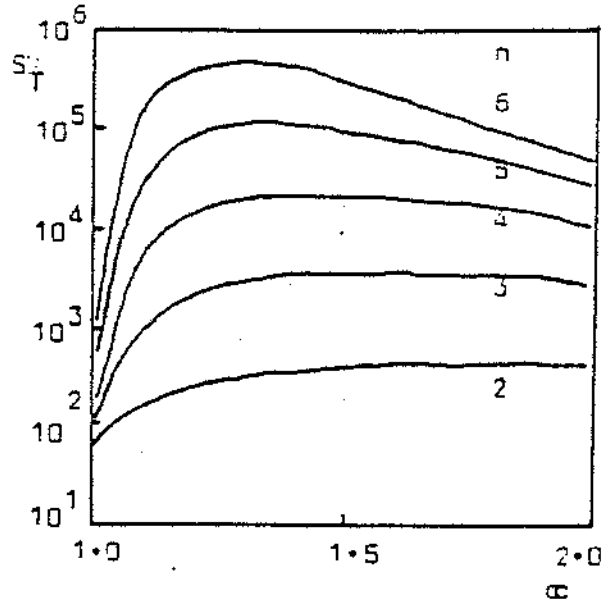

FIG 2·8 : Variation of shielding factor, S_T, with α.

specific example of R_1 = 0·5m, t = 1mm, and μ = 30,000. Although these curves illustrate the behaviour in a specific case, the optimum configuration, in general, will depend on various parameters, i.e. available material, cost, space, etc. One important parameter remains to be calculated in this section, and that is the maximum flux density in the shielding material of the outer layer. It is necessary to know this parameter for two reasons. Firstly, to allow the permeability of the material to be estimated from the relevant μ–B curve, and secondly, to enable some design parameters regarding demagnetisation* to be evaluated.

The flux density in the outer layer will be virtually unaffected by the inner layers, and so a single-layer calculation may be used. Solving 2·6 and 2·7 explicitly for a single layer of high permeability material with thickness t and radius R gives for the trapped flux density, B_m :–

$$\underline{B}_m = \frac{B_o R}{t}\left(\left(1 - \left(\frac{R}{\rho}\right)^2\right)\cos\theta.\hat{\underline{\rho}} - \left(1 + \left(\frac{R}{\rho}\right)^2\right)\sin\theta.\hat{\underline{\theta}}\right) \qquad 2\cdot21$$

This reaches a maximum for $\theta = \pi/2$ when it is completely azimuthal, and for $\rho = R$ equals:–

$$B_m = -\frac{2B_o R}{t} \qquad 2\cdot22$$

From FIG 2·2(b) it can be seen that the assumption, made at the beginning of this section, of a constant permeability through–

* See Section 2·6.

out the shielding material will only be true for $B_m \leqslant .01$ T. In the Earth's field of $\sim 5.10^{-5}$ T this implies $\frac{a}{t} \leqslant 100$ and for layers exceeding this limit some deviations might be expected. However, for a multi-layer assembly, this would only apply to the outer layer.

2·3 Axial magnetic shielding.

Unfortunately no exact solution exists for finite cylindrical magnetic shields in longitudinal fields (see FIG 2·9). The problem must be approached in a significantly different way to that of transverse shielding, in that the axial shielding factor of a single layer is first determined, using magnetostatics, and then extended to multiple layers by a plausibility argument.

2·3·1 Single-layer axial shielding.

In 1968 Mager[29] calculated the axial shielding of a closed cylinder by approximating it to an ellipsoid with minor and major axes corresponding to the length and diameter of the cylinder.

An alternative magnetostatic approach for an exact cylinder is presented here and the results will be shown to be in excellent agreement with those of Mager.

The method separates into two parts:-

(i) the calculation of the flux density distribution at all points within the shielding material, and,

(ii) using this flux density distribution, the field within the shielded region can be found and also a shielding factor.

The overall procedure and assumptions made in each part are outlined below before presenting the detailed calculations.

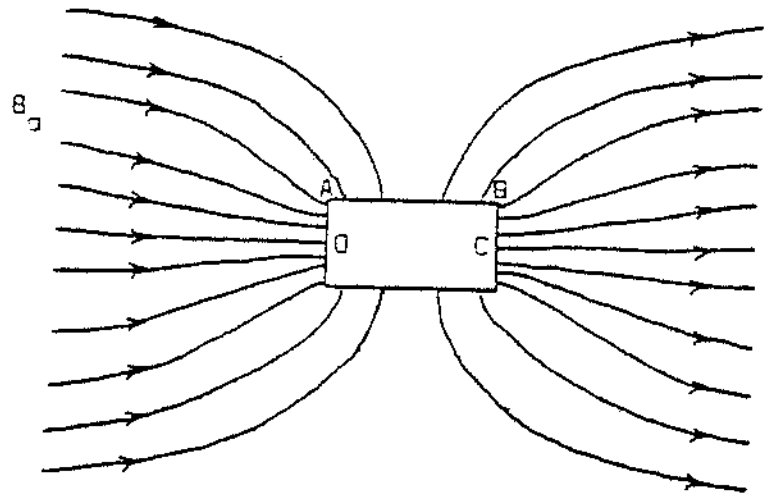

FIG 2-9 : Single-layer axial magnetic shielding.

(i) Leaving two free parameters, to be determined experimentally, a reasonable model for the flux distribution crossing the outside surface of the shielding material is assumed. In the limit of infinite permeability, none of this flux will cross the inner surface (i.e. perfect shielding) and the flux density within the shielding material is then known, except for a normalisation factor. This factor can be found by making the following observation. For the case of perfect shielding ($\mu = \infty$) the magnetic field strength between the centre points of the two end-caps (due to an effective 'magnetic pole density' distribution in the shielding material) must exactly cancel that due to the original unperturbed ambient field. In the case of uniform, as well as infinite, permeability, all the effective magnetic poles will be on the outside surface of the material and, moreover, will be easily determinable from the flux crossing this surface, necessarily normally. This then allows the correct normalisation for the flux density within the shielding material.

(ii) Having calculated the flux density within the shielding material, assuming $\mu = \infty$, the field inside the shielded region must now be found in the real case of finite permeability. This is done by performing the integral $\int \underline{H}.\underline{dl}$ around the closed loop OABC (see FIG 2·9) and assuming the internal field is constant. Again the permeability is assumed uniform.

The calculation will now be presented in detail.

(i) <u>The flux density within the shielding material.</u>

The magnetic field strength, $\underline{H}(r)$, at some point $\underline{r}$, due to a surface magnetic pole density distribution, $\sigma(r')$, is given by

the two following equations:-

$$\underline{H}(r) = -\nabla \phi(r) \qquad 2\cdot 23$$

and

$$\phi(r) = \frac{1}{4\pi}\int_S \frac{\sigma(r')}{|r-r'|}ds \qquad 2\cdot 24$$

where $\phi(r)$ is the magnetic scalar potential at $\underline{r}$ and the integration is over the whole surface, S, holding the magnetic poles. This surface, in the present problem, can be separated into two regions, the end-caps, and the side-walls.
Dealing first with the end-caps, assuming some distribution, $\sigma(\rho)$, for the surface pole density, the total number of magnetic poles on each end-cap will be:-

$$Q_e = \int_0^R 2\pi\rho\sigma(\rho)d\rho \qquad 2\cdot 25$$

and the potential at some point, a distance z away, along the axis due to one end-cap is:-

$$\phi_{e1} = \int_0^R \frac{2\pi\sigma(\rho)\rho}{4\pi(\rho^2 + z^2)^{1/2}}d\rho \qquad 2\cdot 26$$

Adding in the contribution from the other end-cap the potential at the centre of each end-cap due to both end-caps is then:-

$$\phi_e = \pm\frac{1}{2}\int_0^R (1 - \frac{\rho}{(\rho^2 + L^2)^{1/2}})\sigma(\rho)d\rho \qquad 2\cdot 27$$

where L is the length of the shield and $\pm$ sign is for each end-cap. At this point some assumption about $\sigma(\rho)$ must be

made. Taking the two limiting cases of a uniform distribution and one with the same total number of 'poles' around the circumference, 2·27 can be evaluated, for $L > R$, as:-

$$\phi_e = \pm \frac{Q_e}{4\pi R}\left(\left(1 + \frac{1}{4a^3}\right)\beta - \frac{1}{a} - \bigcirc\frac{1}{8a^5}\right) \qquad 2\cdot28$$

where $$\beta = \frac{4\pi R \phi_{e1}(z=0)}{Q_e} \qquad 2\cdot28(a)$$

and $a = L/R$.

The value of the parameter β will depend on the exact form of $\sigma(\rho)$ and may be determined experimentally. Evaluating it for the two limiting cases above gives $2 > \beta > 1$.

Turning now to the side-walls, for a pole distribution, $\sigma(z)$, the potential, ϕ_s, at the centre of either end-cap will be:-

$$\phi_s = \pm \int_0^L \frac{2\pi R\sigma(z)}{4\pi(R^2 + z^2)^{\frac{1}{2}}}dz \qquad 2\cdot29$$

and the total number of poles, Q_s, is:-

$$Q_s = \int_0^L 2\pi R\sigma(z)dz \qquad 2\cdot30$$

Choosing the simplest possible form for $\sigma(z)$ with a linear dependence on z and changing sign half-way along the shield, at $z = L/2$, gives:-

$$\sigma(z) = \sigma_o\left(1 - \frac{2z}{L}\right) \qquad 2\cdot31$$

Introducing another free parameter, α, the constant σ_o, in

2•31 can be related to the average pole density on the end-caps by:-

$$\sigma_o = \frac{\varpi Q}{\pi R^2} e \qquad 2•32$$

Substituting 2•32 and 2•31 into 2•29 and evaluating the integral gives:-

$$\phi_s = \pm \frac{\varpi Q}{2\pi R} e (I_1 - I_2) \qquad 2•33$$

where $$I_1 = \ln(a + (1 + a^2)^{\frac{1}{2}}) \qquad 2•33(a)$$

and $$I_2 = 2((1 + \frac{1}{a^2})^{\frac{1}{2}} - \frac{1}{a}) \qquad 2•33(b)$$

The magnetic field strength between the centre points of the two end-caps is then:-

$$\underline{H} = -\nabla\underline{\phi} = \frac{2(\phi_e + \phi_s)}{L} = \frac{Q_e K}{2\pi R L} \qquad 2•34$$

where $$K = ((1 + \frac{1}{4a^3})\beta - \frac{1}{a} + 2\varpi(I_1 - I_2) + O\frac{1}{8a^5})$$

For $\mu \to \varpi$ this must be equal to the ambient magnetic field strength, H_o, in the absence of the shield. This then gives a value for Q_e of:-

$$Q_e = \frac{2\pi R L H_o}{K} \qquad 2•35$$

Expression 2·35 gives the correct normalisation needed to determine the flux density in the material.

The flux density crossing the outer surface can be related to the surface pole density in the following way. The surface pole density is defined as:-

$$\sigma = \underline{M}.\underline{n} \qquad 2\cdot36$$

where $\underline{M}$ is the magnetisation at the surface and $\underline{n}$ the unit normal to the surface. The assumption of infinite permeability now has two effects. Firstly, $\underline{M}$ becomes equal to $1/\mu_o$ times the flux density, $\underline{B}_m$, inside the material. Secondly, as $\underline{H}_m = 0$ all the flux necessarily crosses the surface normally. Hence the flux density entering the material at any point is simply equal to μ_o times the surface pole density at that point. Under these conditions the total flux density inside the material at any point is μ_o times the integral of all surface poles up to that point divided by the cross sectional area at that point. Of particular interest is the maximum flux density which will occur at the centre point in the side-walls at $z = L/2$ when:-

$$B_m = \frac{\mu_o}{2\pi Rt}\left[\int_0^R 2\pi\rho\sigma(\rho)\,d\rho + \int_0^{L/2} 2\pi R\sigma(z)\,dz\right]$$

$$= \frac{\mu_o H_o L}{K t}\left(1 + \frac{\alpha a}{2}\right) \qquad 2\cdot37$$

(ii) The flux density within the shielded region.

By allowing the material permeability to become finite the

field strength within the material becomes non-zero and the integral $\int \underline{H}.\underline{dl} = 0$ may be performed around the closed loop OABC. Using the flux density distribution determined above, assuming that the internal field strength, H_i, is constant and that the permeability is uniform, this integral is evaluated in Appendix A to give:-

$$B_i = \frac{(1 + \frac{1}{a} + \frac{\alpha a}{3})}{(1 + \frac{\alpha a}{2})\mu} B_m \qquad 2\cdot38$$

where B_m is given in 2·37.

The axial shielding factor then follows:-

$$S^A = 1 + \frac{2K}{a(1 + \frac{1}{a} + \frac{\alpha a}{3})}(\frac{ut}{2R})$$

$$= 1 + \frac{2K}{a(1 + \frac{1}{a} + \frac{\alpha a}{3})} S^T \qquad 2\cdot39$$

The term 1 is added to ensure the right limit as $a \to \infty$, in which case the assumption that all the flux remains in the shielding material becomes non-valid. Therefore, once the parameters α and β have been determined, equation 2·39 gives the axial shielding factor for a single-layer closed cylindrical shield. In the results (Section 2·8), presented later, the 'surface pole' distributions are measured and values of α and β are calculated as 0·85 ± 0·03 and 1·83 ± 0·06 respectively. Using these values the variation of S^T/S^A (assuming $\mu^T = \mu^A$) as a function of a is shown in FIG 2·10. The dotted curve is that calculated by Mager[29]. The close agreement between the two different approaches is remarkable. The crosses are all

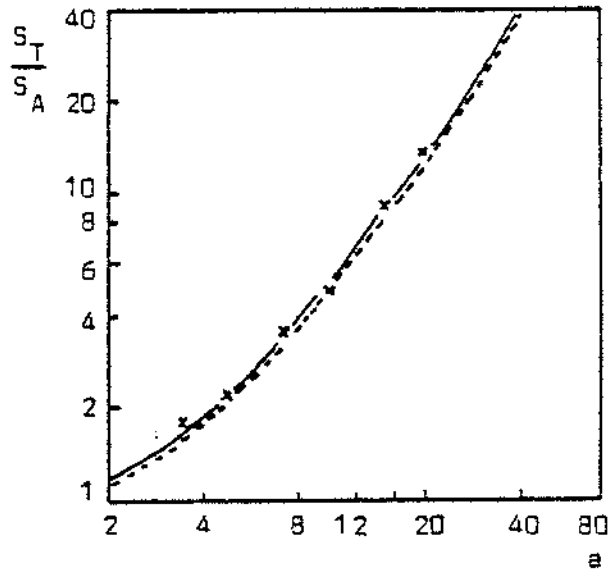

FIG 2•10 : Variation of transverse to axial shielding ratio with the length to radius ratio, a, for a single layer.

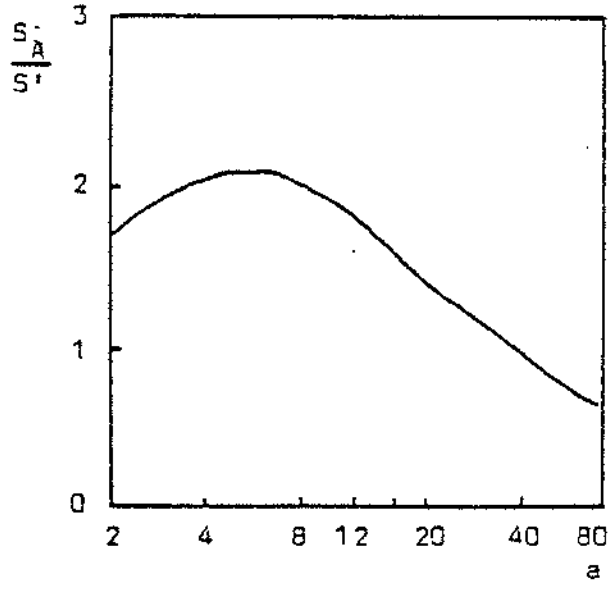

FIG 2•11 : Variation of shielding factor, S_A, with radius assuming a fixed length.

where S^A is the total shielding factor, i.e. :-

$$S^A = S_1^A S_2^A (1 - \frac{L}{L_2}1) \qquad 2\cdot43$$

Allowing $L_2 = L_1$ the shielding factor appears to vanish. Thus the formula is not yet complete. Remembering equation 2·17 for the transverse case a reasonable modification suggests itself:-

$$S^A = S_1^A + S_2^A + S_1^A S_2^A (1 - \frac{L}{L_2}1) \qquad 2\cdot44$$

This now has all the right limits. Equation 2·43 gives the geometric dependence on the lengths of the nested layers and a further examination of equation 2·18 might suggest the generalisation to*:-

$$S^A = \sum_{i=0}^{n} S_i^A + \sum_{i,j>i}^{n-1,n} S_i^A S_j^A (1 - \frac{L}{L_j}i)$$

$$+ \sum_{i,j>i,k>j}^{n-2,n-1,n} S_i^A S_j^A S_k^A (1 - \frac{L}{L_j}i)(1 - \frac{L}{L_k}j)$$

$$+ \ldots + \prod_{i=1}^{n-1} S_n^A S_i^A (1 - \frac{L_i}{L_{i+1}}) \qquad 2\cdot45$$

This formula, for an n-layer assembly, again has all the right limits in the event that any of the lengths are made equal to any other. It will be seen later when this formula is compared with experiment, for some known shielding assemblies, that the

* An article[103] appeared during the final writing of this work using a similar generalisation extending the work of Mager[30].

experimental points taken by Mager except the one at a = 3·5 which comes from this work. If the radius of the shield is kept fixed the curve in FIG 2·10 would also represent the variation of S^A with the length, L, of the cylinder. If, conversely, the length is held fixed then FIG 2·11 shows the variation of S^A with the radius. The quantity S' is defined as $S' = (\frac{\mu t}{2L})$. Thus in a situation where the physical constraint is such that the length of the shield is fixed then there exists an optimum value of the radius to achieve the highest shielding. From FIG 2·11 this occurs for L/R = 5·5.

2·3·2 Multiple-layer axial shielding.

A method will now be proposed for calculating the axial shielding performance of a multi-layer assemoly.

Consider first a double-layer shield where the inner layer is much smaller than the outer, as in FIG 2·12. The field, B'_2, in the absence of the inner layer is:-

$$B'_2 = \frac{B_o}{S_2^A} \qquad 2·40$$

where S_2^A is the axial shielding factor for the outer layer. If the inner layer is now introduced this will partially 'short' the path from A to B and hence:-

$$B_2 = \frac{B'_2 L_2}{(L_2 - L_1)} \qquad 2·41$$

The field inside the inner shield is then:-

$$B_1 = \frac{B_2}{S_1^A} = \frac{B_o}{S_1^A S_2^A (1 - L_1/L_2)} = \frac{B_o}{S^A} \qquad 2·42$$

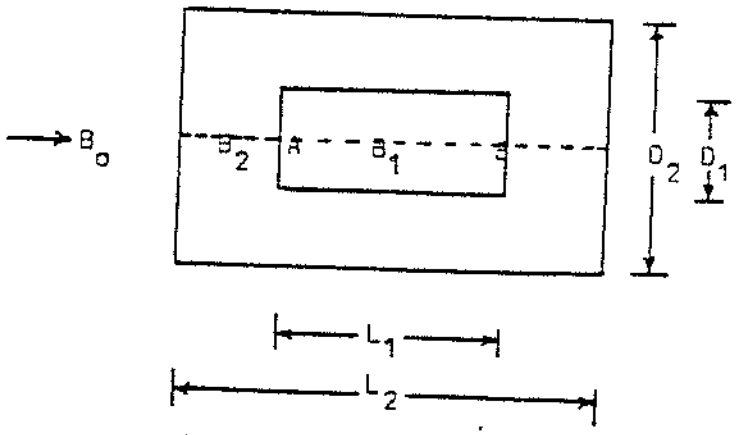

FIG 2·12 : Double-layer axial shielding arrangement.

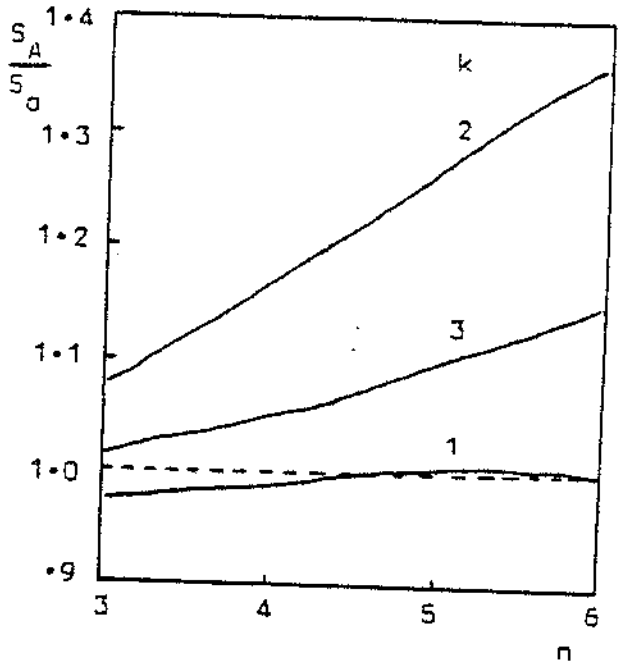

FIG 2·13 : Variation of the multiple-layer shielding factor with k.

agreement is reasonable. An alternative approach using reluctance theory proposed by Pendlebury[50] also gives results in reasonable agreement with 2·45 .

Due to the different geometrical dependance the optimum arrangement for multi-layer shielding, with a fixed amount of material, is no longer a geometrical progression as in the transverse case. In FIG 2·13 is shown the variation of S^A for up to 6 layers taking $L_{i+1} = \alpha^k L_i$ for k=1 to 3 . The dotted line gives the shielding factor which would be obtained with a constant spacing between layers. Of the values tried k=2 gives the highest shielding.

2·4 Open-ended cylinders.

The way in which flux penetrates into an open-ended cylinder can allow some estimate of the effect of holes in the end-caps of closed cylinders. The problem can be solved qualitatively for both transverse and axial configurations as shown in FIG 2·14 . The solution in both cases begins with the general solution for the magnetic scalar potential, ϕ, within the shielded region, in cylindrical coordinates (ρ,θ,z) :-

$$\phi = \sum_{kn} J_n(k\rho)(A_k e^{kz} + B_k e^{-kz})\cos(n\theta) \qquad 2\cdot46$$

(a) Transverse case,

It is reasonable to expect the internal field to have the same angular dependence as the external field, i.e. n=1, in which case:-

$$\phi = \sum_{k} J_1(k\rho)(A_k e^{kz} + B_k e^{-kz})\cos\theta \qquad 2\cdot47$$

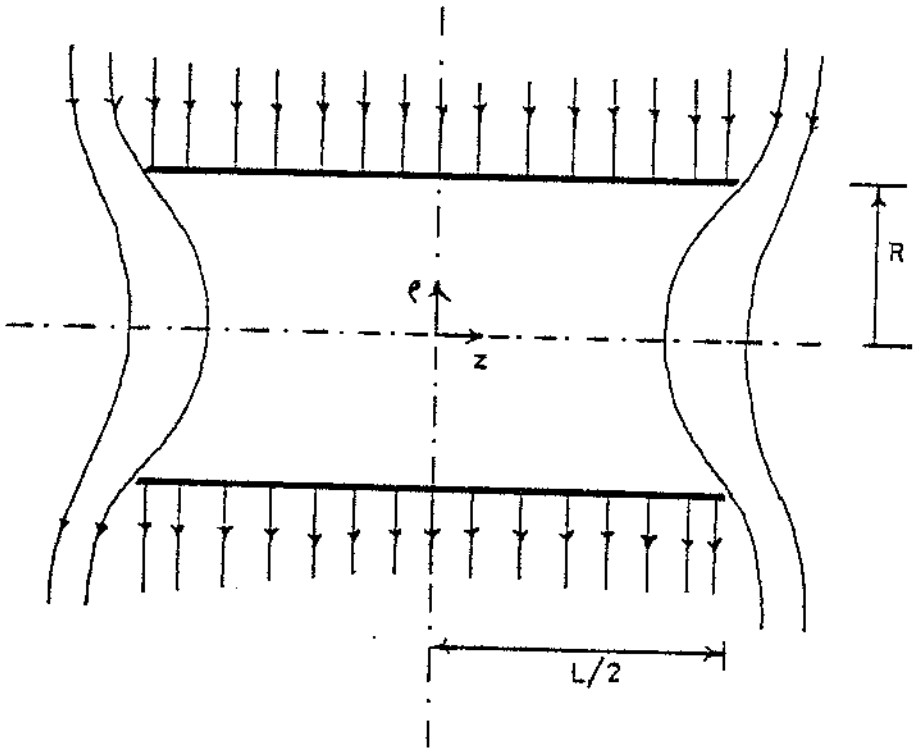

(a) Transverse case.

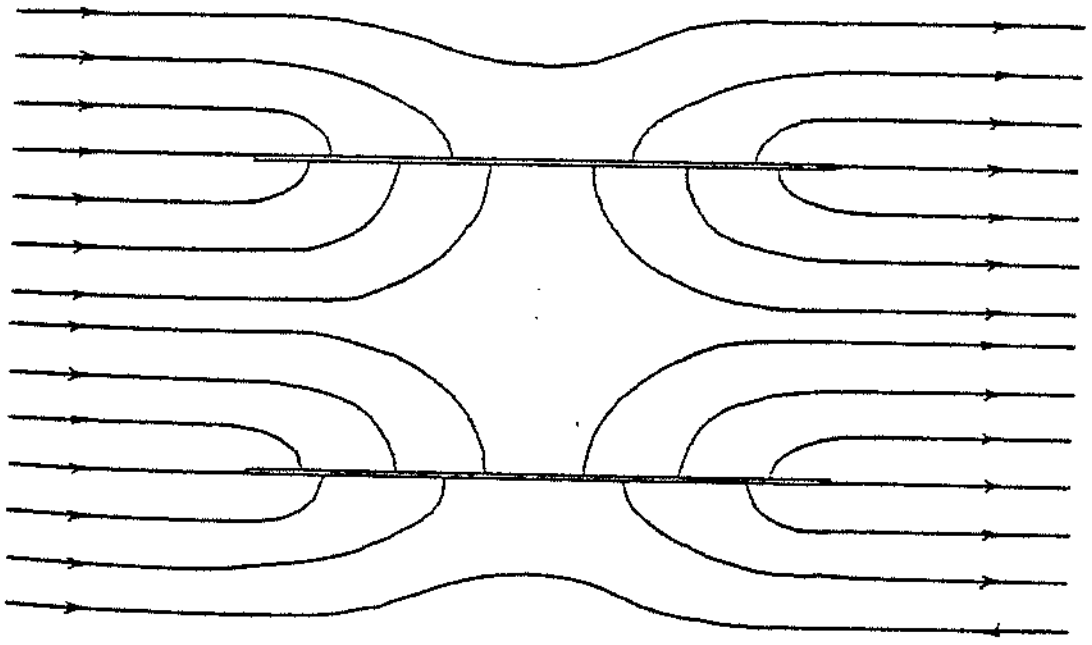

(b) Axial case.

FIG 2·14 : Shielding by open-ended cylinders.

From symmetry the axial field at z=0 must vanish and so $A_k = B_k$ and :-

$$\phi = \sum_k J_1(k\rho)A_k \text{Cosh}(kz)\text{Cos}\theta \qquad 2\cdot48$$

Finally, for high permeability material both the axial and azimuthal field components must go to zero at ρ=R and thus k must be chosen such that $J_1(kR) = 0$. The transverse field within the shielded region is then:-

$$B = -\mu_o \frac{d\phi}{d\rho} = -\sum_k kJ_1'(k\rho)A_k \text{Cosh}(kz)\text{Cos}\theta \qquad 2\cdot49$$

where $J_1(kR) = 0$.

Keeping only the first term it can be seen that the field penetrates approximately exponentially into the shield and, at the centre of the shield, a shielding factor, $S^{T'}$ can be defined as:-

$$S^{T'} = \text{Cosh}\left(\frac{3\cdot83L}{2R}\right) \approx \exp(1\cdot92a) \qquad a>1 \qquad 2\cdot50$$

where a = L/R and 3·83 is the first zero of $J_1(x)$.

For a hole in an end-cap this shielding factor will be further enhanced by the ratio of the field at the hole to that far away.

(b) <u>Axial case.</u>

In this case a similar argument holds except that here there is no angular dependence (n=0) and the radial field must vanish at z = 0. This gives:-

$$B_z = -\sum kJ_o(k\rho)A_k \mathrm{Cosh}(kz) \qquad 2\cdot51$$

where k is such that $J_o(kR) = 0$.

The shielding factor in this case is then:-

$$S^{A'} = \mathrm{Cosh}\left(\frac{2\cdot41L}{2R}\right) \approx \exp(1\cdot2a) \qquad a>1 \qquad 2\cdot52$$

In both the transverse and axial cases this leakage field will be in addition to that expected from the normal shielding factors and a total effective shielding factor, S_{eff} is given by:-

$$\frac{1}{S_{eff}} = \frac{1}{S} + \frac{1}{S'} \qquad 2\cdot53$$

where the suffixes A and T have been omitted.

The problem of a hole in the side-wall of a shield is more complicated as it presents a mixed coordinate system and no attempt is made here to solve this. However some experimental results on this problem are presented later (see Section 2·9).

2·5 Real shielding factors.

In practice exactly what is meant by shielding factor is often unclear because of the non-linear aspects of ferromagnetism. The difficulty is in deciding which permeability is relevant to the specific case being studied. Two situations are commonly met:-

(a) shielding against static fields, and,

(b) shielding against time varying fields.

(a) Static shielding.

In this case the shielding factor is defined simply as the ratio of the external field, far away, to that within the shielded region. For a shield transfered from the furnace to its working position the permeability will depend, in detail, on its magnetic history, and to define a meaningful shielding factor some rigid starting conditions must be assumed. There are two possibilities:-

(i) The magnetic state of the material was originally $B_m = H_m = 0$, and it is suddenly introduced into an external uniform field, B_o. The maximum flux density in the shielding material can be calculated from 2·22 or 2·37 depending on the orientation. From this the permeability is given by the $\mu - B_m$ relationship of the normal magnetisation curve, and is non-linear in B_m. The initial starting conditions $B_m = H_m = 0$ is difficult to achieve in reality and a more easily obtained situation is:-

(ii) By suitably cycling the magnetic state of the material, using a process called demagnetisation (see Section 2·6), the material can be left in a magnetic state corresponding to some point on the anhysteretic magnetisation curve (FIG 2·4), with a flux density again given by 2·22 or 2·37. In this case, for values of B_m away from saturation, the permeability is constant and may be much higher than that in the previous case.

(b) Dynamic shielding.

Here again it is necessary to stipulate the working conditions to be able to define a meaningful quantity and there are two

situations of interest:-

(i) Random quasi-static fluctuations.

Defining the shielding factor as the ratio of the change in the external field, ΔB_o, to the change in the internal field, ΔB_i, from FIG 2·3 it can be seen that, depending on the sign of the disturbance (i.e. either OA or OC in FIG 2·3), the shielding factor can have somewhat different values. Hence in order to have some consistent definition a quasi-static cyclic variation is assumed, when the material will follow a minor hysteresis loop and the effective permeability to use is the incremental permeability. This will be dependant on the size of the perturbation (see equation 2·3 and FIG 2·4(b)), but essentially independant of the ambient magnetic field, B_o. For the EDM experiment, where the time stability of the shielded field is the important quantity, this is the most important shielding factor and unless otherwise stated the term shielding factor will always refer to this quantity in what follows.

(ii) Shielding against periodic variations.

This has been studied by other authors[27,30] and the results are included here for completeness. This shielding factor is always higher than that against quasi-static cyclic variations. FIG 2·15, reproduced from reference (30), shows a typical variation of a parameter, p, with t/δ where t is the material thickness and δ is the skin depth, $(\rho/\pi\mu_o\mu f)^{\frac{1}{2}}$. The a.c. shielding factor is then p times the quasi-static shielding factor of the previous case. For more details the reader is referred to the article by Mager[30] and to the earlier work by Schelkunoff[27]. The results of this section are summarised in

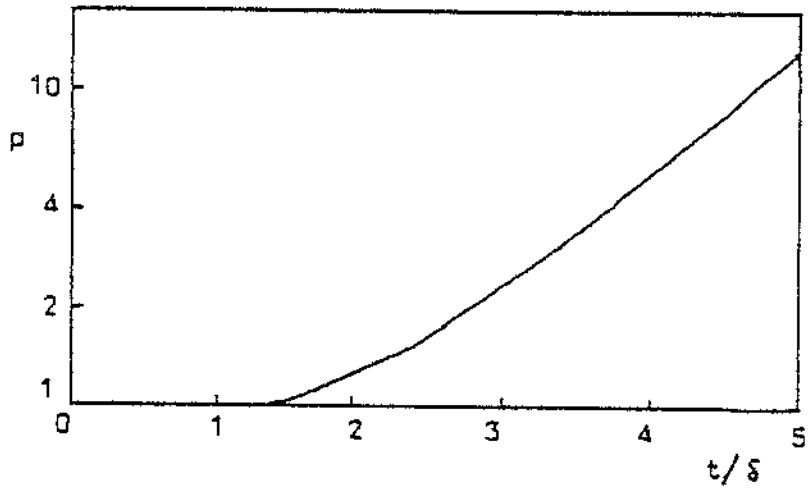

FIG 2·15 : A.C. shielding.

	STATIC		DYNAMIC
	1	2	
μ	30,000	450,000	30,000
Dependence	B_o	-	ΔB_o

1. Before demagnetisation
2. After demagnetisation

Table 2·1 : Some typical permeabilities.

Table 2·1, together with some permeability estimates for mu-metal assuming a low flux density within the material.

2·6 Demagnetisation.

Demagnetisation is the name given to any means of manipulating the magnetic state of the material onto the anhysteretic curve. This can be done in three ways:-

(a) the most common means of applying a large alternating magnetic field to the sample and gradually reducing it to zero,

(b) heating the sample above its Curie temperature (~390°C for mu-metal) in the ambient field and slowly cooling it to room temperature, or,

(c) mechanically shocking the sample in the ambient field.

Method (a) is the simplest choice and is usually achieved by passing an alternating current through a central conductor along the axis of the shield[51]. The magnetic field strength within the material is then:-

$$H_m = \frac{NI}{2\pi R} \qquad 2·54$$

where NI is the total current and R the shield radius.

This field strength must initially be enough to saturate the shielding material and must be allowed to decay to a value less than that due to the gathered flux from the ambient field. For a transverse ambient field, B_o, this will be (from 2·22) :-

$$H_m = \frac{2H_o R}{\mu t} \qquad 2·55$$

It is interesting to note, from an experimental point of view

this method of demagnetisation is equally effective for both transverse and longitudinal directions.

2·7 Shaking.

'Shaking' is a procedure whereby the shielding factor against low frequency perturbations can be enhanced by the application of a suitable a.c. 'shaking' field[28,52].

In 1967 Cohen[52] noted that the shielding factor appears to be enhanced for frequencies both above and below the 'shaking' frequency, but was unable to explain either convincingly. In what follows a model is presented which allows an estimation of of the enhancement to be expected at low frequencies.

For the 'shaking' procedure to be effective the 'shaking' field must be large enough that the high permeability region of the magnetisation curve is approached. This is represented in FIG 2·16 by the hysteresis loop CC'. The tips of this loop lie on the normal magnetisation curve and its reflection in the third quadrant. Dealing first with perturbations at much lower frequencies than the 'shaking' frequency, consider a change in the external field which produces a change ΔB in the flux density in the shielding material. The hysteresis loop CC' then becomes DD', as shown in FIG 2·16 by the dotted line. The effective permeability for this shift is simply equal to the slope of the line joining the extremities CC' (or DD' for small ΔB) of the loop. As long as the ambient static field is not large enough to significantly offset the hysteresis loop from the centre, this slope is given, to a good approximation, by the permeability calculated from the normal magnetisation curve at the tip C of the loop. Using this argument the maximum

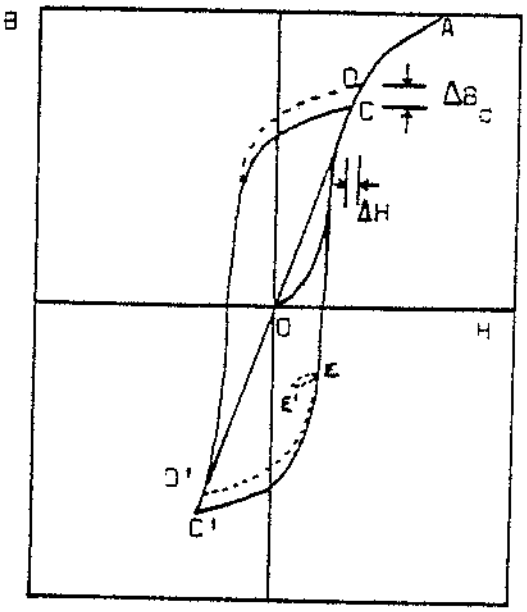

FIG 2·16 : Large hysteresis loop used for 'shaking'.

enhancement which could be expected would be the ratio of the maximum permeability to the initial permeability, and this would occur for a 'shaking' field amplitude just sufficient to reach the turn-over point on the normal magnetisation curve. Hence, in the case of Cohen[52] who used 4-79 permalloy, the maximum enhancement would be ~5 and would occur at H_s ~4 A/m (from FIG 2·1(a)). In practice he saw an enhancement of 3 at 4 A/m. One of the reasons why he did not achieve a factor of 5 is that he used a short open-ended cylinder and the leakage into the cylinder from the ends (according to equation 2·50) would certainly have been enough to lower the apparent enhancement significantly. Correcting for this gives an enhancement of ~4·2.

For perturbations at higher frequencies than the 'shaking' frequency minor hysteresis loops, such as EE' in FIG 2·16, would be expected, and hence no enhancement, or suppression, of the shielding factor would occur. When the perturbing frequency is comparable to the 'shaking' frequency the situation obviously becomes more complicated. However, it seems probable that some enhancement will still occur (albeit to a lesser extent) for perturbing frequencies up to, say, a factor of 3 above the 'shaking' frequency. For a perturbation frequency 2½ times the 'shaking' frequency Cohen saw an enhancement of 1·5. In fact, on time scales comparable to the 'shaking' period, some modulation (or beating) of the apparent shielding factor may be seen.

In practice 'shaking' frequencies around 50 Hz have been used. In the specific case of the EDM shield this could well cause

problems in itself as the envisaged transition frequency for the neutron magnetic resonance will be only 30 Hz.

2·8 The prototype magnetic shield.

The motivation for building a prototype multi-layer shield was twofold. Firstly, to test some of the predictions of shielding theory, and secondly, to provide a magnetically quiet region for testing the sensitive optically pumped rubidium vapour magnetometer. Thus, shielding factors of 10^5 – 10^7 were aimed at, being high enough to provide a sufficiently quiet region for the magnetometer, but low enough to measure. The length to radius ratio was chosen to be similar to that thought necessary for the final assembly, and the length of the inner layer enough to accomodate the magnetometer. This resulted in a 4-layer assembly of about $\frac{1}{3}$ of the size of the final design. A schematic drawing of the assembly is shown in FIG 2·17. The shielding material used was 1·57 mm mu-metal, and all other parts were of aluminium alloy. All the shielding layers consisted of a cylinder with two detachable end-caps. As it is well known that any stress may be detrimental to the magnetic properties[48 p595ff], the design allowed for each cylinder to be supported independently at both ends around the whole of the inner circumference. This allowed for a minimum of stress to be present in the shielding material with the assembly in the horizontal position, and also ensured that the weight of each cylinder was transmitted directly to the supporting frame, and not via any other cylinder. This also allowed any combination of layers to be mounted on the main frame. The rig was assembled vertically and then, if necessary, pivoted about

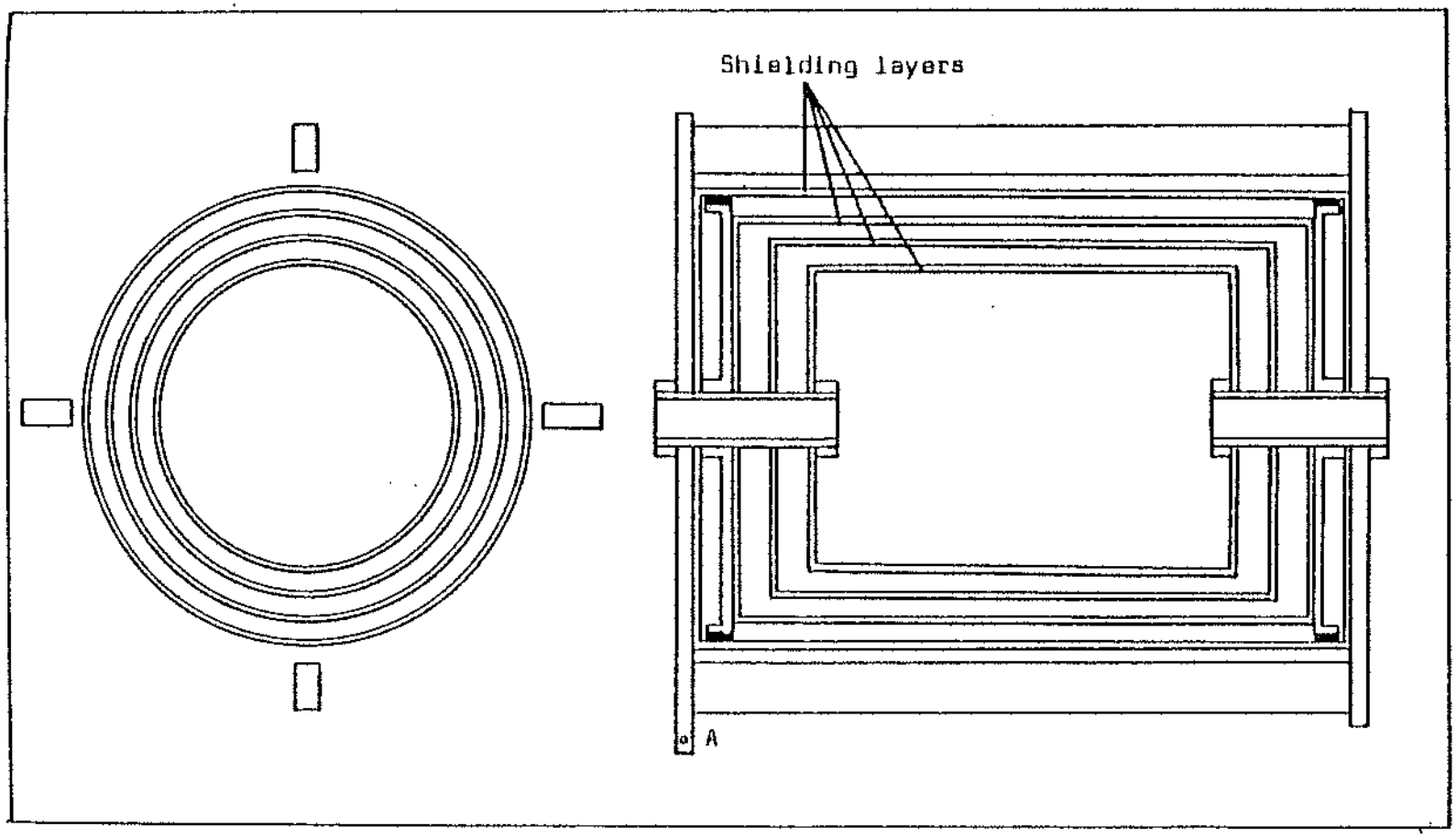

FIG 2•17 : The prototype magnetic shield design.

point A (see FIG 2·17) into the horizontal position. Hence the four very substantial external struts. The assembled rig is shown in the vertical position in Plate 1. Also visible is some of the electronics for the magnetometer. The overall dimensions of each layer were as follows:-

1. ·150, ·530 ; 2. ·175, ·620 ; 3. ·200, ·710 ; 4. ·225, ·800 .

The two numbers are the radius and length respectively in metres. A constant spacing in both the radial and longitudinal directions was used to facilitate construction and assembly. Using these dimensions and assuming a permeability of 30,000, equations 2·15, 2·18, 2·39, and 2·45 predict, for a perfect assembly, axial and transverse shielding factors of $1 \cdot 1.10^5$ and $3 \cdot 4.10^6$ respectively. There were two other important design features incorporated in the prototype shield. Firstly, there appeared to be two firms[53] in England capable of manufacturing the final assembly. However the heat-treatment[54] of mu-metal is crucial to its magnetic properties, and whilst one of the firms (Telcon Metals) only had a relatively small hydrogen furnace but guaranteed a very high permeability (~50,000), the other firm had a large hydrogen furnace but could not give any estimate of the resulting permeability. Hence it was decided to obtain half of the assembly from each manufacturer. The inner and outer layers were ordered from Magnetic Shields, whilst the middle two, each necessarily in three pieces, were ordered from Telcon Metals. The inner layer was kept as a completely welded cylinder in order to avoid any possible inhomogeneity problems arising from bad joints. Secondly, it was highly probable that in the final assembly some of the

joints would have to be made in the transverse sense and so an overlap joint was included on the outer layer in the hope of gaining some experience in this type of joint. This is clearly seen in Plate 1. The joints in the middle two layers were in the longitudinal sense and arranged as shown in FIG 2·18. The dural clamps were machined to a radius matching that of the mu-metal and home-made dural bolts were used (commercial brass bolts were found to contain too much ferromagnetic impurity and produced unpredictable results when demagnetising). Overlaps on all end-caps were 5 cm.

In order to measure some shielding factors, two large orthogonal square coil pairs were constructed around the shield as shown in FIG 2·19. One produced axial fields and the other transverse fields. The whole assembly was positioned such that the Earth's field lay in the vertical plane through the shield axis. Thus fields could be applied to add or subtract to either (or both) components of the Earth's field. The fields produced by each coil pair was calculated using the Biot-Savart law for each straight section and then summing over all such sections. Using 6 turns on each coil and with 14 amps available from the circuit of FIG 2·20, a maximum field of $\cdot 4.10^{-4}$ T was achievable. The switch S_1 allowed small variations to be superimposed on the applied steady field.

The next piece of equipment required was some means of demagnetising the shields. A field strength > 10 A/m is needed to saturate mu-metal and so for the outer shield with R = ·225 m equation 2·54 implies a total current >14 amps is required. This must be allowed to decay to <·025 amps, assuming

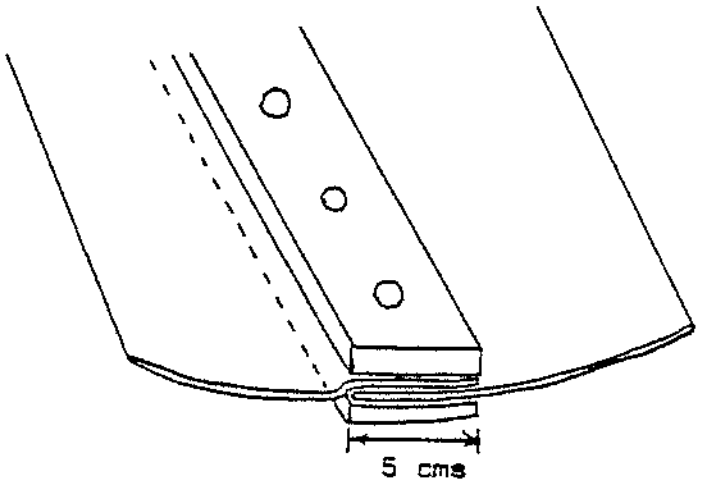

FIG 2•18 : Longitudinal overlap joints used on the middle two layers.

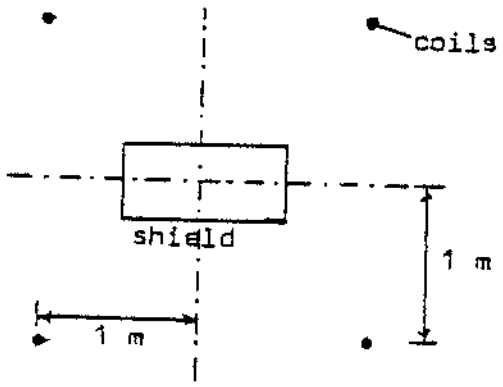

FIG 2•19 : External field coils.

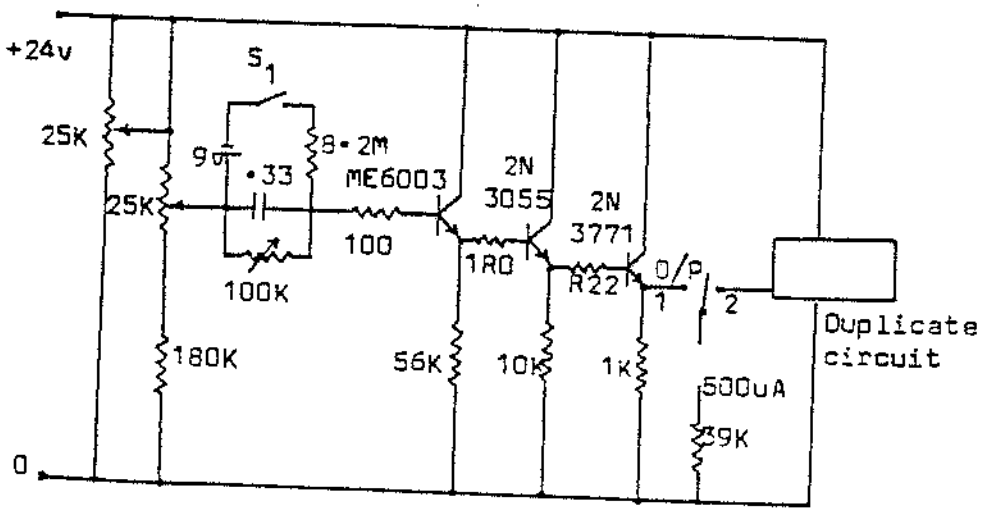

FIG 2•20 : External field coil power supply.

$B_o \approx 5.10^{-5}$ T and $\mu \approx 450{,}000$ is the permeability of mu-metal on the anhysteretic magnetisation curve, estimated from FIG 2·1(b). This corresponds to an attenuation factor 560. Usually the current is drawn from a mains powered circuit operating at 50 Hz. However, as the skin depth in mu-metal is only ·32 mm at 50 Hz (assuming μ = 30,000), it was decided to design an electronic circuit capable of supplying up to 60 amps at a variable frequency (5 to 60 Hz), and also to control the demagnetising routine. The final circuit is shown in FIG 2·21. An internal oscillator decides the frequency. The rms output voltage is compared to the d.c. output from an integrator unit, and an error voltage is produced which keeps these two voltages equal by altering the shunt resistance of an fet transistor operating as a voltage variable resistor. If a voltage is now applied to the input of the integrator such that the integrator output ramps towards zero, then the rms voltage at the current output will follow it. The initial starting current and the decay time could be varied from the front panel. The decay time was variable from 30 secs to ~10 mins. An attenuation factor ~6000 was obtained. By far the most critical adjustment necessary was to ensure that there was no d.c. current present, although by purposefully applying some d.c. bias, whilst demagnetising, the final magnetic state of the mu-metal could be manipulated as required.

2·9 Results.

This section divides naturally into three parts. The first is concerned with the behaviour of the shielding factors and comparison with theory for some known shielding assemblies.

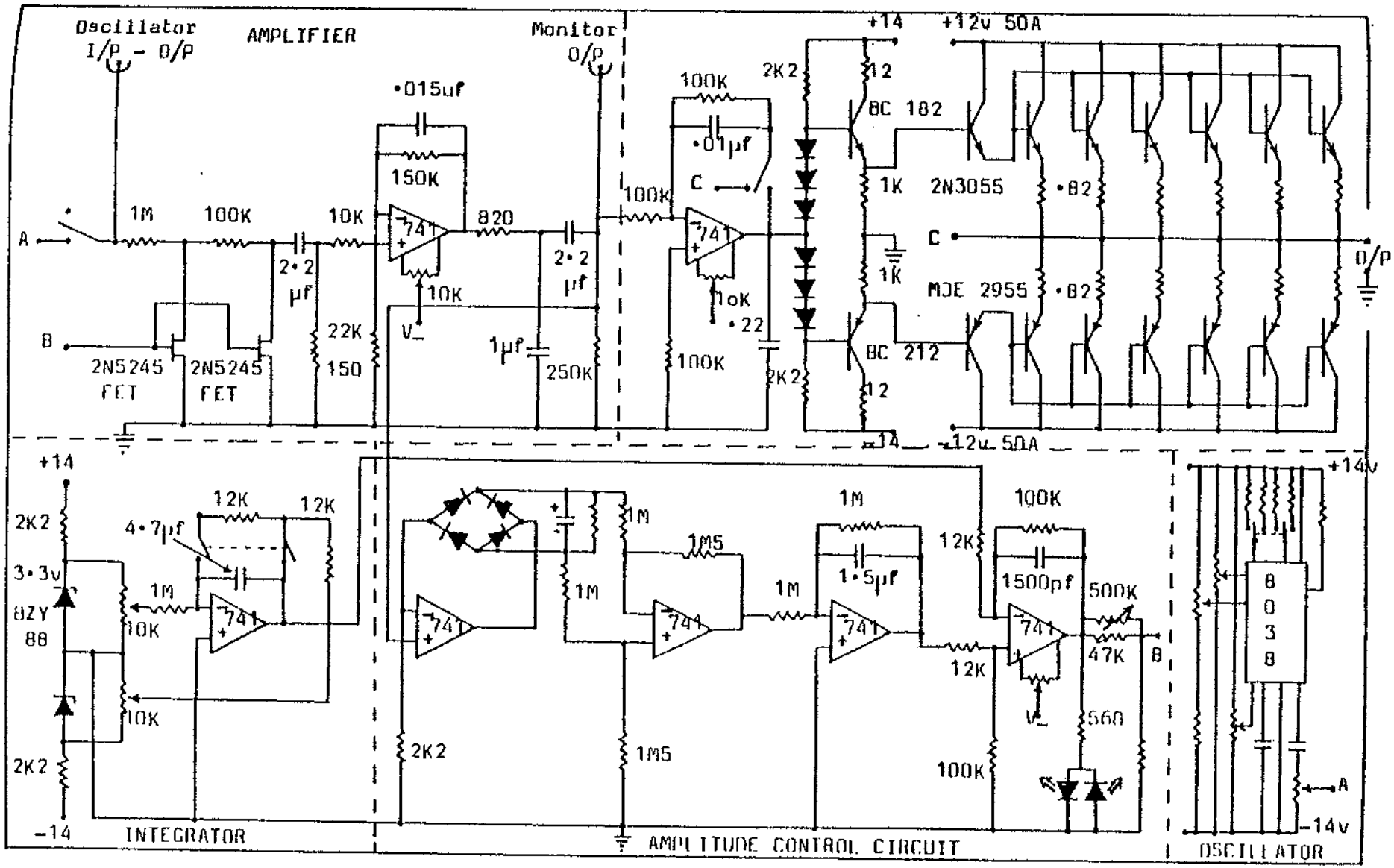

FIG 2•21 ; Demagnetising circuit.

The second part deals with the flux penetration through holes, field variation along the axis, remnant fields after demagnetisation etc., and finally, in the third part, the effect of clamping joints as shown in FIG 2·18.

(a) Behaviour of shielding factors.

There were four points which seemed worthy of some investigation under this heading;

(i) the determination of α and β for use in the single-layer axial shielding calculations,

(ii) are the multi-layer shielding performances adequately described by equations 2·18 and 2·45 ?,

(iii) do the shielding factors vary in agreement with equation 2·3 as the size of the perturbation amplitude is changed ?, and,

(iv) are the shielding factors really independent of the ambient field strength, H_o, as implied by FIG 2·5(a).

(i) Determination of α and β.

Recalling the argument of Section 2·3·1, the value of depends on the distribution of the 'magnetic pole' surface density over the end-caps. For $\mu \gg 1$ this is equivalent to the distribution of the normal flux density, B_n, over the surface of the end-cap. This was easily measured (see FIG 2·22) using a commercial flat transverse Hall probe (RFL Universal Gaussmeter Model 3265). The inner layer of the prototype was used for these measurements and was positioned in a purely axial field $\sim 3.10^{-5}$ T.

Looking at FIG 2·22 the increase in the flux density for small r is due to a 5·5 cm diameter hole at the centre of the

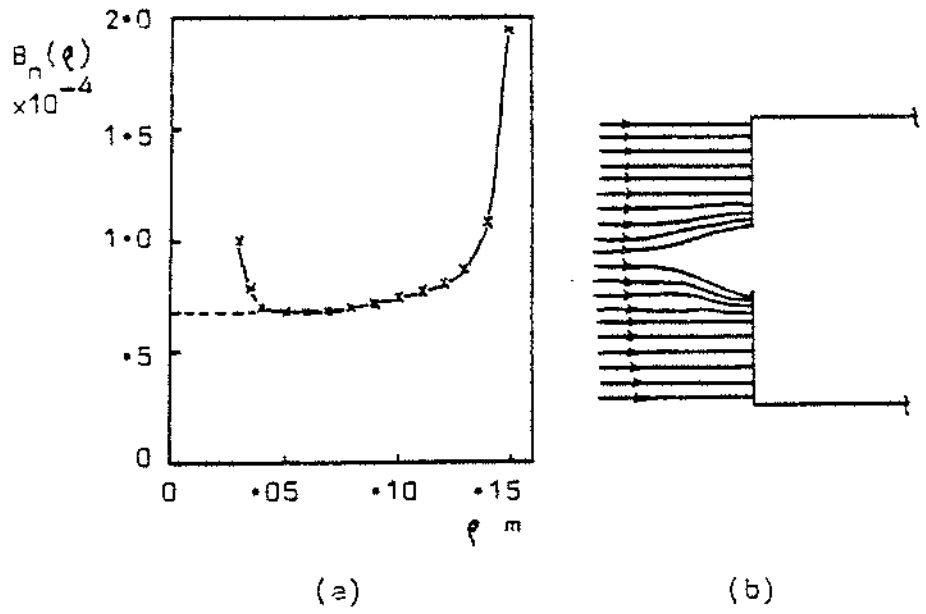

FIG 2·22 : Normal flux density distribution over the end-cap.

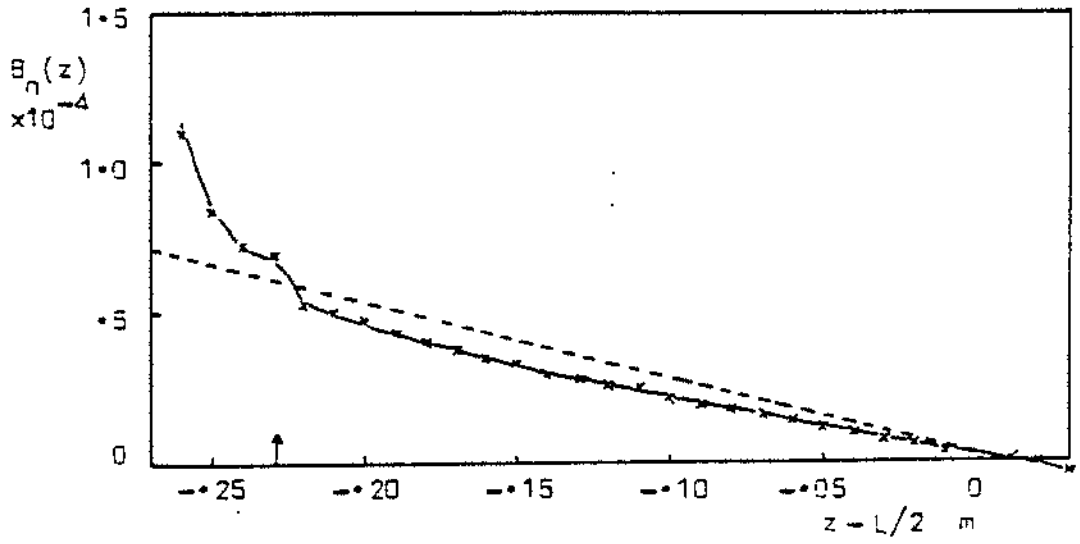

FIG 2·23 : Normal flux density distribution along the side-wall.

end-caps. This would have the effect shown in FIG 2·22(b), and so an increase would be expected. In fact a direct calculation shows that the integrated flux density (i.e. the total flux) contained above the dotted line exactly equals that which would have entered the missing disc. The dotted line curve is used for the calculation of β. Remembering 2·28(a) the value of β is given by:-

$$\beta = \frac{4\pi R \phi_e}{Q_e}$$

where $$Q_e = \int_0^R 2\pi\rho\sigma(\rho)d\rho = \int_0^R 2\pi\rho \frac{B_n(\rho)}{\mu_o} d\rho \qquad 2\cdot56(a)$$

and $$\phi_e = \int_0^R \frac{2\pi\sigma(\rho)}{4\pi} d\rho = \int_0^R \frac{2\pi B}{4\mu_o} n\frac{(\rho)}{\pi} d\rho \qquad 2\cdot56(b)$$

From the experimental data (see FIG 2·22(a)) it is found:-

$$\mu_o Q_e = (599\cdot1 \pm 7\cdot4)\times10^{-8} \text{ Weber}$$

and $$4\pi\mu_o\phi_e = (72\cdot9 \pm 1\cdot4)\times10^{-6} \text{ Tm}$$

from which $$\beta = 1\cdot83 \pm 0\cdot06 \qquad 2\cdot56(c)$$

Similarly the value of α can be determined from the normal flux density distribution along the side-wall of the shield, again keeping a purely axial external field. The measured distribution is shown in FIG 2·23. It was assumed in the theory that the surface 'pole' density distribution along the side-walls was linear. Away from the region of the end-cap

overlap (arrowed) this seems to have been a reasonable assumption. The dotted line represents a linear variation of the surface 'pole' density having the same area under the curve, i.e. the same number of poles. The intercept then gives the effective value of the distribution at the end-cap, i.e. σ_o. Hence:-

$$\mu_o\sigma_o = (7{\cdot}2 \pm 0{\cdot}2)\times10^{-5}\ T$$

Then $\alpha = \pi R^2\sigma_o/Q_e$ which gives, using the value of Q_e above:-

$$\alpha = 0{\cdot}85 \pm 0{\cdot}03$$

(ii) Variation of shielding factor with ΔB_o.

In FIG 2·24 are shown the results of some measurements of this variation for the transverse shielding. They were performed using the outer layer of the prototype shield. The field variations were applied using the external field coils. The results were then least-squares fitted to a curve of the form (cf equation 2·3) :-

$$S^T = \frac{ut}{4R}(1 + (1 + CD\Delta I)^{\frac{1}{2}}) \qquad 2{\cdot}57$$

where $D\Delta I = \Delta B$ and $C = 4\nu/(\mu_1\mu_o)^2$.

The solid lines in FIG 2·24 represent the 'best fit' curves. The second (lower) set of data was taken after the shield had been assembled and disassembled several times and shows a 25% degradation in shielding factors. The parameter D relates the

average flux density in the shielding material to the μA reading on the meter of FIG 2•20, and involves three terms. These are the relations between the μA reading and the external field, the external field to the maximum flux density in the material, and the maximum flux density to the average flux density, such that:-

$$D = (7{\cdot}90.10^{-7}) \times (\frac{2R}{t}) \times (\frac{2}{\pi})$$

where 2R/t comes from equation 2•22 and $2/\pi$ is the result of the average of flux density over all angles using 2•21.
For the largest shield, with R = 0•225 m and t = 1•57 mm, this gives $D = 1{\cdot}44.10^{-5}$. The least-squares fit for the upper set of data then gives:-

$$(CD) = (3{\cdot}42 \pm 0{\cdot}32)\times 10^{-3} \text{ and } \mu_1 = 46{,}950 \pm 570$$

Hence $C = 237{\cdot}3 \pm 22{\cdot}2$ and $\nu = 0{\cdot}207 \pm 0{\cdot}024$

For the lower set of data:-

$$(CD) = (2{\cdot}60 \pm 0{\cdot}78)\times 10^{-3} \text{ and } \mu_1 = 35{,}010 \pm 570$$

Hence $C = 180{\cdot}4 \pm 54{\cdot}1$ and $\nu = 0{\cdot}087 \pm 0{\cdot}029$

The parameter ν clearly seems to be a function of the initial permeability, μ_1.
Although it would be untrue to say that equation 2•57 has been

verified (in that a straight line would also give a reasonable fit to the data), it is fair to say that, over the range of $\Delta I(\Delta B)$ considered, there is no significant disagreement. Hence equation 2•57, together with the values of the parameters obtained here, will be used to normalise shielding factors taken using different field changes.

(iii) Multiple-layer shielding factors.

In Table 2•2 are shown the measured and corresponding theoretical shielding factors for various known shielding assemblies. Measurements with the prototype shields were done by applying a known external field change, in a cyclic manner, and then measuring the resultant change inside the shielded region. All measurements, unless otherwise stated, were done with a fluxgate magnetometer (RFL Model 101) with a sensitivity of 5.10^{-10} T. Where possible, all values have been corrected to try to allow for the variation in shielding factor with the magnitude of the applied field change, as described in the previous subsection.

The results show a worst case disagreement of a factor of ~3 for the axial shielding performance of Taran's prototype (T1), although his measurement procedure was somewhat dubious. For his final assembly (T2), on which a different measurement procedure was used, there is much better agreement. Both of Taran's assemblies were run with the outer end-cap missing and so the two values quoted are for a comolete assembly with all end-caps and for an assembly without the outer layer. The real performance would be expected to lie between these two extremes. The reasonable agreement for these large assemblies

SHIELD	n	EXPERIMENTAL S_T	EXPERIMENTAL S_A	THEORY S_T	THEORY S_A
P1 *	1	152 ± 24	73 ± 2	–	78 ± 12
P2	1	61 ± 4	46 ± 2	–	–
P3	1	53 ± 2	38 ± 2	–	–
P4	1	163 ± 16	54 ± 4	–	–
P14	2	19,980 ± 4990	2200 ± 160	14,120 ± 4170	1638 ± 175
P24	2	3,760 ± 180	780 ± 19	4,172 ± 750	738 ± 91
P34	2	2,370 ± 70	457 ± 7	2,024 ± 300	360 ± 46
P134	3	152,500 ± 76,250	4,444 ± 250	143,220 ± 43,130	8,120 ± 1135
P1234	4	5.10^5	89,890 ± 4,350	$(1{\cdot}42 \pm {\cdot}55).10^6$	40,710 ± 7,010
OR *	2	200	16	–	18 ± 1
T1	6	8,530	450	$1{\cdot}44.10^6$	1,040 – 2320
T2	5	10^5	240	$2{\cdot}84.10^5$	230 – 380
F	2	–	100 ± 10	[illegible]	119 **
EDM	5	10^5	$1 - 3.10^4$	5.10^5	$1{\cdot}1.10^4$

Table 2·2 : Multiple-layer shielding factors (see explanatory notes on following page).

Pn : prototype shield layers as designated by n.

OR : Oak Ridge shield as used in references (8) and (36).

T1 : Taran's prototype[47]. Note this 6-layer assembly only used 5 end-caps and the two values for S_A(theory) are for 5-layer and 6-layer assemblies respectively. The true value would lie somewhere between the two.

T2 : Taran's final assembly[50]. This 5-layer assembly only had 4 end-caps and so two values are again given for S_A(theory). The quoted permeability for the material of this shield was 48,000, whereas 52,000 was claimed for the prototype, T1.

F : Shield belonging to M. Forte and being used in a parity violation experiment involving neutron spin rotation[39].

EDM : EDM final assembly (see Section 2·10).

* S_T(exp) used to estimate μ and hence predict S_A.

** μ = 20,000 assumed.

All theoretical predictions for the prototype are based on the single layer performances, and have been corrected for effects of the type 2·57.

is encouraging as these provide a reasonable test of the theory.

Hence it would appear that equations 2•18 and 2•45 are able to adequately predict the shielding properties of multi-layer assemblies. In particular equation 2•45 allows, apparently for the first time*, an estimation of the axial shielding performance of multi-layer systems.

(iv) Variation of shielding factors with the steady applied field magnitude.

These measurements were done by passing a constant current through the external field coils in addition to the cyclic variation. The external field is then the sum of the applied field and the Earth's field. The inner layer of the prototype was used and the results are shown in FIG 2•25 (page 62) for both axial and transverse cases. No significant variation is seen.

(b) Remnant fields.

On first positioning the inner layer of the prototype assembly in a constant external field of $0•31.10^{-4}$ T ($0•099$ & $0•291 \times 10^{-4}$ T axial and transverse respectively) the axial and transverse remnant fields inside at the centre were $1•8.10^{-7}$ T and $0•53.10^{-7}$ T respectively. As the detailed magnetic history of the shield was not known, these numbers cannot be related to a meaningful shielding factor. The variation of both of these field components, along part of the length of the shield, on axis, is shown in FIG 2•26 (curves 1 & 2 are the transverse

* See footnote page 38.

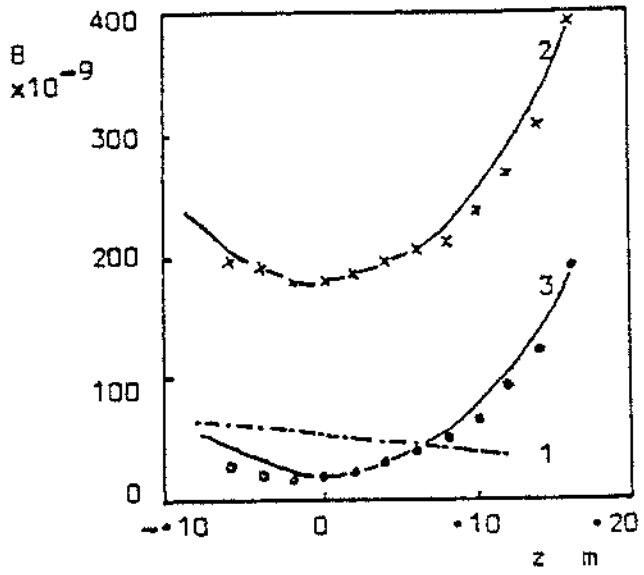

FIG 2·26 : Remnant magnetic fields.

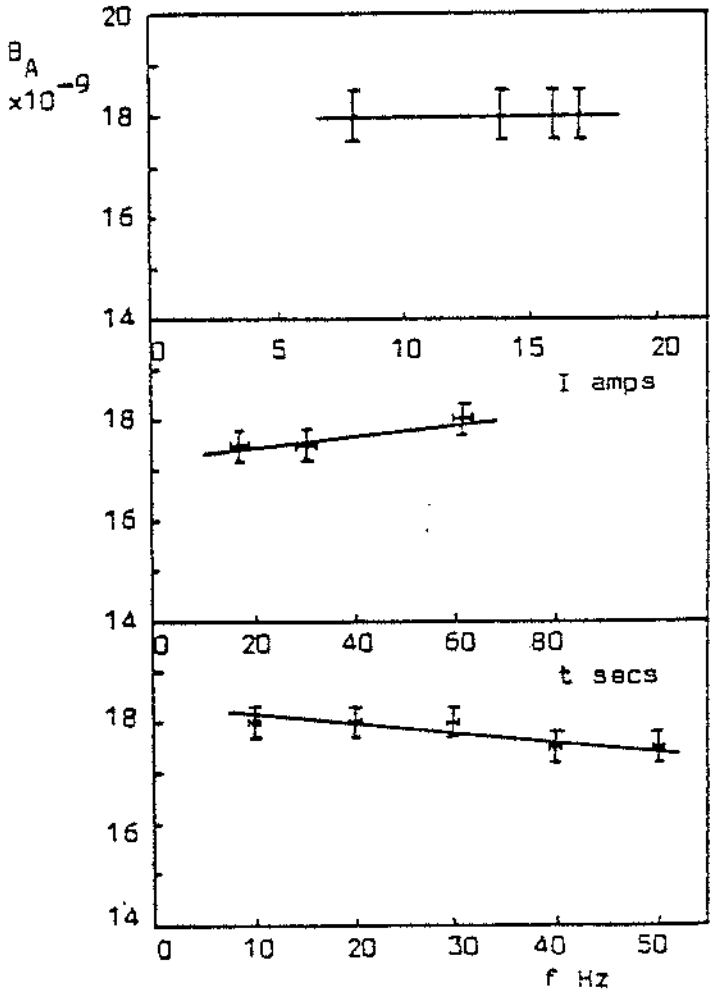

FIG 2·27 : Effect of demagnetisation parameters.

and axial components respectively). The transverse field was everywhere parallel to the external transverse field component. The variation of the axial field is attributed to flux penetration through a 5 cm diameter hole in each end-cap. This is supported by curve 3 in FIG 2·26 which shows the axial field variation after demagnetising. From Section 2·4 the variation expected would be:-

$$B_a(z) = B_{ao} + B'_a \exp(\frac{kz}{R}) \qquad 2·58$$

where B_{ao} is the remnant field given by B_o/S^A and S^A is the shielding factor described in Section 2·5(a)(i), but with an arbitrary starting condition. B'_a is the axial field at the centre of the holes in the end-caps, and k = 2·405 is the first zero of the Bessel function $J_o(k)$.

The solid lines on curves 2 & 3 are fitted at points z = 0 and z = 16 cm. These give:-

$$B'_a = 1·75.10^{-8} \text{ and } 1·42.10^{-8} \text{ respectively, and,}$$

$$B_{ao} = 1·63.10^{-7} \text{ and } 5·8.10^{-9} \text{ respectively.}$$

Extrapolating back to the end-caps, the field at the centre of the holes would be $1·2.10^{-6}$ T, i.e. 12% of the external field. The residual field, B_{ao}, after demagnetisation is $\sim 6.10^{-9}$ T. This would imply a permeability $\sim 590{,}000$ which is in reasonable agreement with the previous estimate of $\geqslant 450{,}000$ using FIG 2·1(b). The value of S'_a is almost

independent of the demagnetising procedure (and hence the effective permeability). This is again consistent with it being associated with leakage through the holes. Varying the external field, the ratio $B_a(0)/B_o$, after demagnetisation, was found to be constant at 0·0022. Hence there is a field at the centre of the shielded region due to flux leakage which must be allowed for in any comparison between experimental and theoretical shielding factors. For the inner layer this field, $B'_a = 0{\cdot}00148_o$, corresponded to an apparent shielding factor of 697. The relationship between the measured shielding factor and the true ideal shielding factor is:-

$$\frac{1}{S_{exp}} = \frac{1}{S} + \frac{1}{697} \qquad 2{\cdot}59$$

The correction turns out to be ~10% and, allowing for this, the predicted ratio of transverse to axial shielding factors agrees with experiment to 8%. However, in the analysis of the shielding performances earlier the measured values were used. The transverse field, after demagnetisation, was $\sim 3.10^{-9}$ T. However this field was extremely sensitive to any d.c. offsets in the demagnetising current, and indeed, could be adjusted in this way to almost any value. The axial remnant field was fairly insensitive to d.c. offsets as the demagnetising field is purely azimuthal and hence orthogonal* to the axial fluxes. Thus a d.c. offset does not produce an asymmetry in the way

* It is interesting to note that demagnetisation using a central conductor is equally effective in both axial and transverse directions.

that it does for the transverse case. Owing to the highly sensitive behaviour of the transverse remnant field component, all subsequent demagnetisation measurements were done in the axial direction. FIG 2·27 shows the variation of the axial remnant field with some of the demagnetisation parameters. Between each of the points the magnetic state of the shield was cycled to leave it in an undemagnetised state. From the results the demagnetisation procedure appears to work over a large range of parameters. In particular only 85 A/m (8 amps through 10 turns) was required.

Following this the transverse flux penetration through holes in the side-walls of a single-layer shield was investigated. In FIG 2·28 are shown the results of such measurements, using two different sized layers of the prototype shield, each with two different sized holes. Curves 1 & 3 are for the smallest layer (R = 0·15 m) with hole radii, r_h, of 1·1 and 1·9 cm respectively. Curves 2 & 4 are for the largest layer (R = 0·225 m) with the same hole radii. Within the shield the flux appears to penetrate exponentially. Fitting these portions of the curves to straight lines gives, for the penetration constants, k_i, assuming a penetration as $\exp(k_i \rho)$:-

$$k_1 = 1{\cdot}277 \pm 0{\cdot}065 \text{ and } k_3 = 0{\cdot}713 \pm 0{\cdot}028$$

$$k_2 = 1{\cdot}498 \pm 0{\cdot}001 \text{ and } k_4 = 0{\cdot}840 \pm 0{\cdot}040$$

From these results it appears that k scales as $1/r_h$ but seems almost independent of R. Hence the effective shielding factor

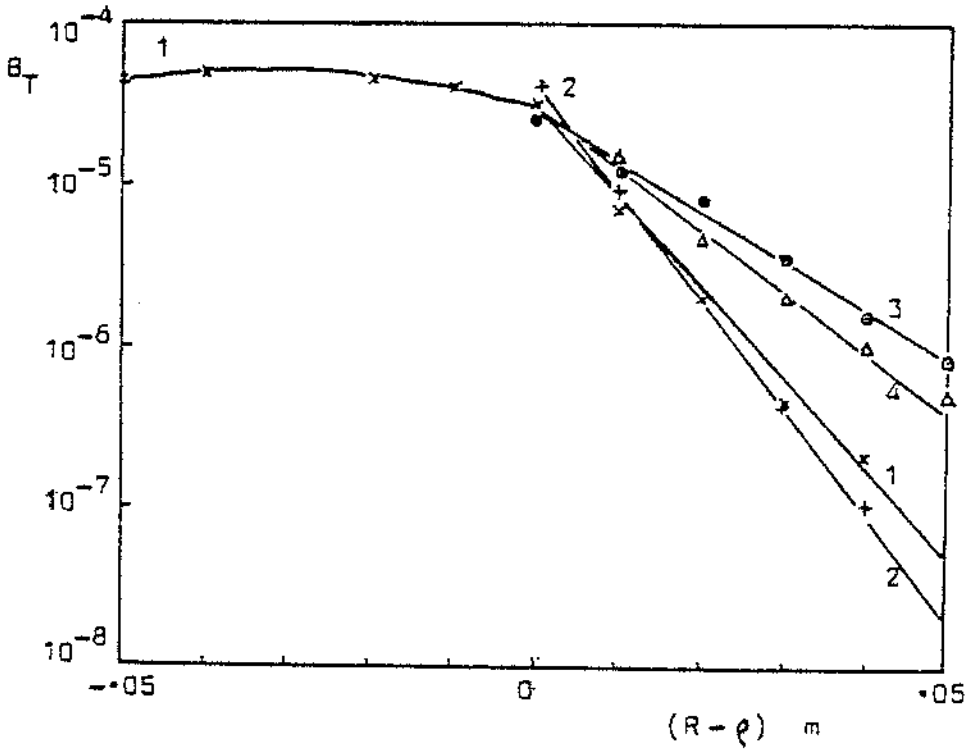

FIG 2·28 : Transverse field penetration through side holes.

for this type of leakage could be rewritten as:-

$$S = \exp\left(\frac{kR}{r_h}\right) \qquad 2\cdot60$$

where $k \approx 1\cdot5$.

For the smallest layer of the prototype this would give $S \approx 140{,}000$ for the largest hole. This is a negligible correction in this work.

(c) Effect of joints.

It can be seen from Table 2·2 that some of the ratios of the transverse to axial single-layer shielding factors depart significantly from the factor of 1·8 predicted theoretically. This was attributed to the presence of joints in all but the first layer. The two middle layers, with longitudinal joints, as shown in FIG 2·18, suffered reductions of 22% and 31% in their transverse shielding factors. The outer layer, with a joint in the transverse sense, suffered a reduction of 34% in its axial shielding factor.

2·10 A design for the final EDM shield.

In Section 1·2 it was shown that to achieve an EDM sensitivity of 5.10^{-28} m, consistent with the UCN counting statistics, the absolute field must be stable to better than 10^{-11} T over each switching period of the electric field, ~30 s. The experiment will be performed in an applied field, B_o, of 10^{-6} T, which means that, parallel and perpendicular to B_o, field fluctuations must be $< 10^{-11}$ T and $< 4.10^{-9}$ T respectively. The field, B_o, will be produced transversely inside the shield (see FIG 1·3) to take advantage of the intrinsically higher

shielding factors obtainable in this direction, and, assuming typical laboratory ambient field fluctuations $\sim 10^{-7}$ T, transverse and axial shielding factors of $> 10^4$ and > 25 are required respectively. Allowing for possible improvements in the available UCN flux, permitting a better EDM sensitivity, and a reasonable safety margin, shielding factors of 10^6 and 10^4 in the transverse and axial directions respectively were aimed at.

Fixing the inner and outer radii at 1 m and 2 m respectively, and assuming a permeability of 40,000 (comparable to the outer layer of the prototype), a 5-layer assembly was decided upon with the following dimensions:-

1. 1·000, 1·404 ; 2. 1·156, 1·636 ; 3. 1·346, 1·934;

4. 1·580, 2·300 ; 5. 1·936, 2·740 .

The two numbers are the diameters and lengths respectively in metres. The radii of the three inner layers were reduced slightly, from the optimum geometrical progression, to allow them to be heat-treated as complete sections. The cylindrical sections of the outer two layers were made in as few pieces as possible to minimise the effects of joints. All layers have detachable end-caps at both ends. The inner three layers are in 2 mm thick material while the outer two are in 1·57 mm material. Assuming a permeability of 40,000 for the three inner layers but only 20,000 for the outer two (allowing for the joints) , equations 2·18 and 2·45 give shielding factors of $1{\cdot}1.10^6$ and 4.10^4 for the transverse and axial directions. Measurements on the permeabilities, using the method of

Appendix A, of the individual sections during construction* gave disappointingly low values as shown in FIG 2·29. Using the average permeability values shown in FIG 2·29, which attempt to allow for the effect of joints, the estimates for the transverse and axial shielding factors become 5.10^5 and $1{\cdot}1.10^4$ respectively. Preliminary measurements, using a flux-gate magnetometer, have given the real shielding factors as $> 10^5$ and $(2 \pm 1)\times 10^4$.

Due to the overall size of the assembly some consideration was given to the problem of stresses in the mu-metal lowering its permeability. In reference (49) is found a statement that a stress of $7{\cdot}5.10^5$ N/m^2 produces a degradation of ~30% in the permeability of permalloy. Assuming a similar figure holds for mu-metal, calculations on the deformation and stresses induced in horizontal cylinders showed that, for the inner layer, which would sag ~ ·02 m under its own weight, the actual sag should be kept to less than 2.10^{-4} m. For this purpose thick dural rings were placed at intervals around the outside of each layer and provided the main frame assembly (see Plate 2).

Holes of 20 cm and 10 cm diameter are required, diametrically opposite, in the centre of the side-wall of each layer to allow the entry of the neutron guide tube and the high voltage cable respectively. The effect of these holes can be estimated using equation 2·60 to give:-

* Constructed at Magnetic Shields, Staplehurst, Kent.

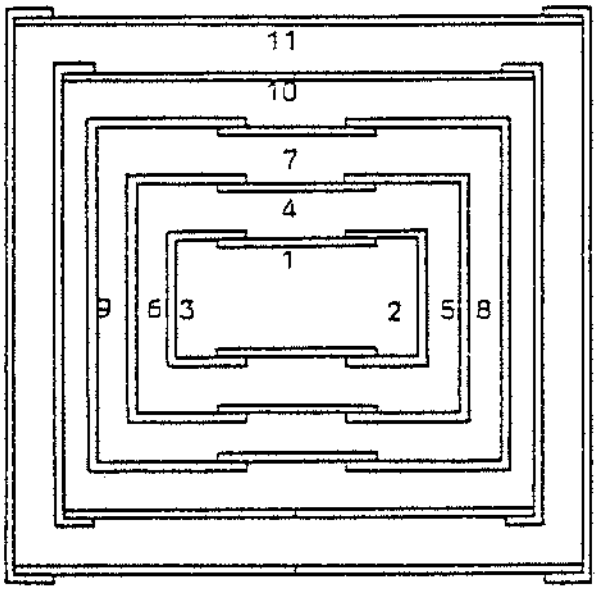

Shield 1 : 1. 19,000 2.36,000 3. 27,000

Shield 2 : 4. 24,000 5. 36,000 6. 31,000

Shield 3 : 7. 18,000 8. 28,000 9. 28,000

Shield 4 : 10. 20,000

Shield 5 : 11. 22,000

FIG 2·29(a) : Measured permeability values for individual sections of the final EDM shield.

SHIELD	μ_T	μ_A
1	28,000	22,000
2	30,000	25,000
3	28,000	21,000
4	20,000	20,000
5	22,000	22,000

FIG 2·29(b) : Average permeabilities taken for each layer.

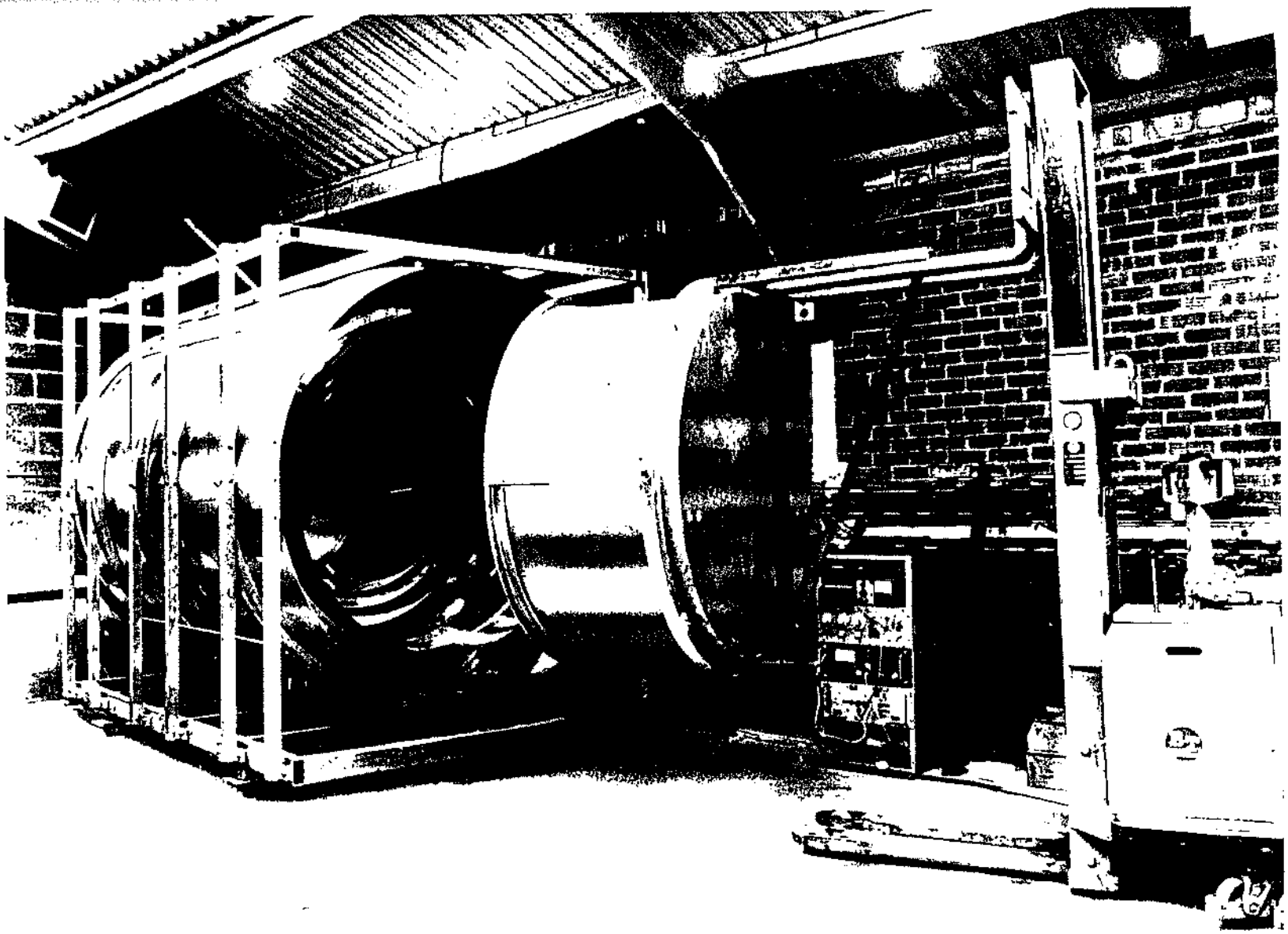

$$\frac{1}{S_h} = \frac{1}{S_{h1}} + \frac{1}{S_{h2}} \approx \frac{1}{2.10^6}$$

for a single layer of 1·936 m diameter. The way in which the inner layers enhance this shielding, if at all, is not clear, but even without any enhancement this shielding factor is acceptably high.

2·11 Superconducting shields.

To achieve EDM sensitivities much less than 10^{-28} m will necessitate superconducting shielding. Two basic properties of superconductors contribute to their shielding performance. These are the Meissner effect and zero resistance or infinite conductivity. The first property relates to the static shielding and the latter to the dynamic shielding. The transition to the superconducting state results in all magnetic flux being excluded from the material. This is the Meissner effect and for a closed superconducting shell should provide a field free region inside the shell. However, in practice, due to impurities, dislocations, etc., the Meissner effect is never complete. Several tricks may be used to overcome this problem, such as, mu-metal outer layer(s), nested superconducting shields cooled sequencially from the outside inwards, spinning the shield as it is cooled to convert static fields to dynamic fields, and opening out originally folded superconducting 'sacks'.

Dynamic field changes are shielded by induced surface currents flowing in a layer ~500 Å thick. Any varying fields penetrate exponentially so that as long as the shield is several times

thicker than ~500 Å the shielding should be extremely high for a single layer.

Recent reviews of superconducting shielding are given in articles by Hamilton[55].

For the EDM experiment an open-ended cylinder may be preferred to a closed shell as a closed shell greatly enhances the field inhomogeneities of any internally generated fields (see Appendix A).

REFERENCES.

1. GOLUB R. & PENDLEBURY J.M. : Rep. Prog. Phys. 42,439,(1979)
2. STEYERL A. : Springer Tracts in Mod. Phys. 80,57,(1977)
3. LUSCHIKOV V.I. : Phys. Today 30,42,(1977)
4. GOLUB R. et al. : Sci. Am. 240,106,(June 1979)
5. DRESS W.B. et al. : Phys. Rev. D 15,9,(1977)
6. ALTAREV I.S. et al. : LINP 430 (1978) Leningrad Inst. Phys. Conf. Ser. 42,179,(1978)
7. BYRNE J. et al. : Rutherford Proposal 157 (1974)
8. DRESS W.B. & MILLER P.D. : Inst. Phys. Conf. Ser. 42,11,(1978)
9. LEE T.D. & YANG C.N. : Phys. Rev. 104,254,(1956)
10. WU C.S. et al. : Phys. Rev. 105,1413,(1957)
11. LANDAU L. : Nucl. Phys. 3,127,(1957)
12. CHRISTENSON C.J. et al. : Phys. Rev. Lett. 13,138,(1964)
13. SCHUBERT K.R. et al. : Phys. Lett. 26B,11,(1970)
14. GOLUB R. & PENDLEBURY J.M. : Cont. Phys. 13,519,(1972)
15. RABI I.I. : Phys. Rev. 51,652,(1937)
16. RAMSEY N.F. : Molecular Beams, OUP (1956)
17. HANSON R.J. & PIPKIN F.M. : Rev. Sci. Inst. 36,179,(1964)
18. della PORTA : Magiae naturalis, sive de miraculus rerum naturalium Libri VII (1589)
19. RUCKER A.W. : Phil. Mag. 37,95,(1894)
20. WILLS A.P. : Phys. Rev. 9,193,(1899)
21. STERNE T.E. : Rev. Sci. Inst. 6,324,(1935)
22. WALKER L.R. : Rev. Sci. Inst. 6,416,(1935)
23. WADEY W.G. : Rev. Sci. Inst. 27,910,(1956)
24. CRAVATH A.M. : Rev. Sci. Inst. 28,559,(1957)
25. SCHWEIZER A.W. : J. APP. Phys. 33,1001,(1962)

26. ESMARCH W. : Ann. Physik 39,1540,(1912)

27. SCHELKUNOFF S.A. : Bell Sys. Tech. J. 13,532,(1934)

28. ALBACH W. & VOSS G.A. : Z.Angew Phys. 9,111,(1967)

29. MAGER A.J. : J. App. Phys. 39,1914,(1968)

30. MAGER A.J. : IEEE Trans. Mag. MAG-6,67,(1970)

31. KLEPPNER O. et al. : Phys. Rev. 138,A972,(1965)

32. PATTON B.J. & FITCH J.L. : J. Geophys. Res. 67,1117,(1962)

33. COHEN D. : J. App. Phys. 38,1295,(1967)

34. COHEN D. : Rev. de Phys. App. 5,53,(1970)

35. COHEN D. : Phys. Today 28,34,(1975)

36. GREENE G.L. et al. : Phys. Lett. 71B,297,(1977)

37. DUPONT-ROC J. et al. : Phys. Lett. 28A,638,(1969)

38. COHEN-TANNOUDJI C. et al. : Phys. Rev. Lett. 22,758,(1969)

39. RAMSEY N.F. : Phys. Rep. 43C,409,(1978)

40. TARAN Y.V. : JINR P3-7377 Dubna (1974)

41. TARAN Y.V. : JINR P3-7785 Dubna (1974)

42. ALEKSEEV N.A. et al. : JINR P13-9221 Dubna (1975)

43. TARAN Y.V. : JINR P13-9275 Dubna (1975)

44. NIKITENKO Y.V. & TARAN Y.V. : JINR P13-10067 Dubna (1976)

45. NIKITENKO Y.V. & TARAN Y.V. : JINR P13-10068 Dubna (1976)

46. TARAN Y.V. : JINR P3-7147 Dubna (1973)

47. TARAN Y.V. : JINR P3-7149 Dubna (1973)

48. BOZORTH R.M. : Ferromagnetism, Van Nostrand (1951)

49. RAYLEIGH LORD. : Phil. Mag. 23,225,(1887)

50. PENDLEBURY J.M. : Private communication (1977)

51. HERRMANNSFELDT W.B. & SALSBURG B.L. : Rev. Sci. Inst. 35,906,(1964)

52. COHEN D. : App. Phys. Lett. 10,67,(1967)

53. TELCON METALS Ltd. : CRAWLEY, SUSSEX.

MAGNETIC SHIELDS. : STAPLEHURST, KENT.

54. See for example :- MUMETAL ALLOYS : TP11-874,58,(1974)

Telcon Metals Ltd.

55. HAMILTON W.O. : Meth. Exp. Phys. 11,609,(1974)

Rev. de Phys. App. 5,41,(1970)

56. PACKARD M. & VARIAN R. : Phys. Rev. 93,941,(1954)

57. SKILLMAN T.L. & BENDER P.L. : J. Geophys. Res. 63,513,(1958)

58. STUART W.F. : Rep. Prog. Phys. 35,803,(1972)

59. KASTLER A. : J. Phys. et Rad. 11,255,(1950)

60. BALLING L.C. : Adv. Quant. Elec. 3,1,(1975)

61. HAPPER W. : Rev. Mod. Phys. 44,169,(1972)

62. FRANZEN W. & EMSLIE A.G. : Phys. Rev. 108,1453,(1957)

63. HAWKINS W.B. : Phys. Rev. 123,544,(1961)

64. HAWKINS W.B. : Phys. Rev. 182,39,(1969)

65. DEHMELT H.G. : Phys. Rev. 105,1487,(1957)

66. BOUCHIAT M.A. & BROSSEL J. : Phys. Rev. 147,41,(1966)

67. FRANZ F.A. & FRANZ J.R. : Phys. Rev. 148,82,(1966)

68. BARRAT J.P. & COHEN-TANNOUDJI C. : J. Phys. et Rad.

22,329,443,(1961)

69. COHEN-TANNOUDJI C. : Ann. de Phys. 7,423,469,(1962)

70. BOUCHIAT M.A. : J. de Phys. 26,415,(1965)

71. COHEN-TANNOUDJI C. et al. : Rev. de Phys. App. 5,95,102,(1970)

72. DEHMELT H.G. : Phys. Rev. 105,1924,(1957)

73. BELL W.E. & BLOOM A.L. : Phys. Rev. 107,1559,(1957)

74. WHITE C.W. et al. : Phys. Rev. 174,23,(1968)

75. BOUCHIAT M.A. : Publ. Sci. Tech. Min. Air, France, Notes

Tecn. 146,(1965). Thesis (1965) Paris.

76. BOUCHIAT M.A. : J. de Phys. 24,379,511,(1963)

77. HERMAN R.M. : Phys. Rev. 136,A1576,(1964)

Phys. Rev. 137,A1062,(1965)

78. KILLIAN T.J. : Phys. Rev. 27,578,(1926)

79. GROSSETETE F. : J. de Phys. 25,383,(1964)

J. de Phys. 29,456,(1968)

80. WATANABE S.F. & ROBINSON H.G. : J. Phys. B 10,931,959,(1977)

J. Phys. B 10,1167,(1977)

81. WATANABE S.F. et al. : J. Phys. B 10,941,(1977)

82. SYKES J. : J. Phys. B 10,1151,(1977)

83. PEGG D.T. : J. Phys. B 6,241,(1973)

84. BROSSEL J. et al. : C.R. 237,984,(1953)

85. WINTER J.M. : C.R. 241,375,600,(1955)

86. BROSSEL J. et al. : C.R. 241,556,(1955)

87. BELL W.E. et al. : Rev. Sci. Inst. 32,588,(1961)

88. BREWER R.G. : Rev. Sci. Inst. 32,1356,(1961)

89. GERARD V.B. : J. Sci. Inst. 39,217,(1962)

90. SMITH K.F. : Private communication. (1978)

91. IGNATOVICH V.K. & TEREKOV G.I. : JINR P4-10548 Dubna (1977)

92. EGOROV A.I. et al. : Sov. J. Nucl. Phys. 19,147,(1974)

93. LOBASHEV V.M. et al. : LINP 37 (1974) Leningrad.

94. LUSCHIKOV V.I. et al. : JINR P3-4127 Dubna (1968)

JETP Lett. 9,23,(1969)

95. GROSHEV L.V. et al. : Phys. Lett. 34B,293,(1971)

96. FRANK I.M. : JINR P3-9846 Dubna (1976)

97. BYRNE J. : Private communication. (1978)

98. STEYERL A. : Z. Physik 254,169,(1972)

99. GALLOP J.C. & RATCLIFFE W.J. : J. Phys. D 11,L203,(1978)

100. TINKHAM M. : Introduction to superconductivity ,
M^{C}Graw Hill,(1975)

101. GIFFARD R.P. et al. : Prog. Quant. Elec. 6,301,(1976)

102. RAMSEY N.F. : Private communication (1979)

103. GUBSER D.U. et al. : Rev. Sci. Inst. 50,751,(1979)

104. SMYTHE W.R. : Static and dynamic electricity ,
M^{C}Graw Hill,(1950)

Appendix A

(a) Permeability measurements.

These were done using a standard magnetic induction technique. Three coils were wound around the sample as shown in FIG A1. The first was for demagnetising, the second as a drive coil, and the third the pick-up coil. The voltage induced in the pick-up coil is simply:-

$$V = - N\frac{d\phi}{dt} \qquad A1$$

where N is the number of turns. The flux, ϕ, is related to the current, i, in the drive coil by:-

$$\phi = \frac{ni}{R'} \qquad A2$$

where n is the number of drive turns and R the reluctance of the magnetic circuit which is given by:-

$$R = \int_l \frac{1}{\mu A} dl \qquad A3$$

where l is the flux path. Measurements were done essentially at d.c. by manually switching the current, i. The voltage, V, was then integrated to give:-

$$V_o = \int V dt = - \frac{nNi}{R'} \qquad A4$$

Two shapes of most interest were cylindrical shells and end-caps with holes in the centres. The reluctances of these two

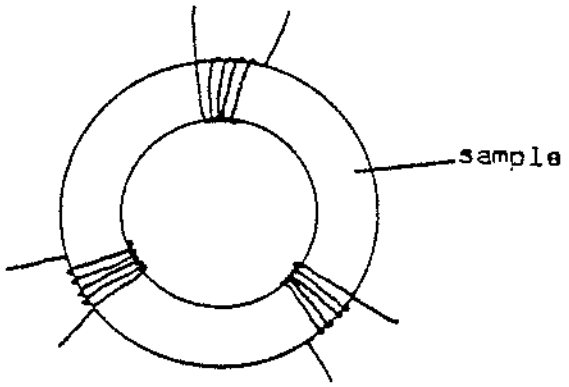

FIG A1 : Magnetic circuit for permeability measurements.

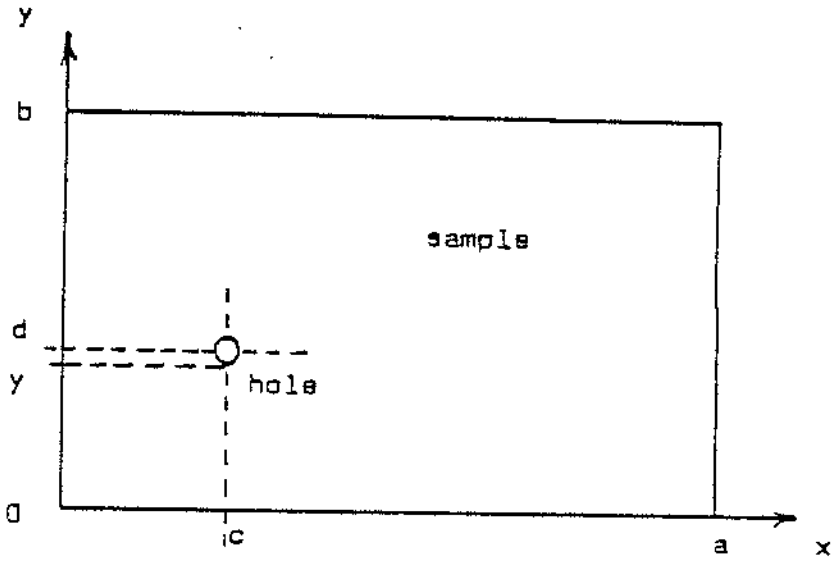

FIG A2 : Rectangular sample dimensions.

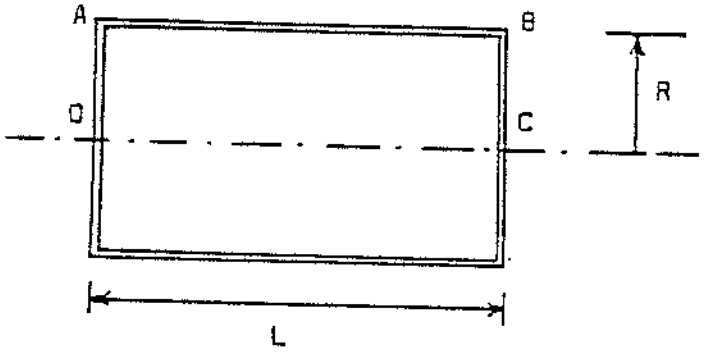

FIG A3 : Single layer shield.

shapes are:-

$$R'(\text{cyld}) = \frac{2\pi R}{\mu t L}$$

$$R'(\text{end-cap}) = \frac{2\pi}{\mu t}\left(\frac{1}{\ln(R/r_1) + 1/R}\right) \qquad \text{A5}$$

where r_1 is the hole radius in the centre of the end-cap, and l is the skirt length. The permeability has been assumed constant throughout the material.

A third shape which was used was a rectangular section with a hole at some position (see FIG A2). In this case[104]:-

$$R' = \frac{\pi}{2\mu t}\sum_{m=1}^{\infty}\frac{1}{m}\text{Cosech}\left(\frac{m\pi b}{a}\right)\text{Sinh}\left(\frac{m\pi(b-d)}{a}\right)\text{Sinh}\left(\frac{m\pi y}{a}\right)\text{Sin}^2\left(\frac{m\pi c}{a}\right) \qquad \text{A6}$$

(b) Axial shielding - Relationship between h_i and H_{max}.

Consider FIG A3. Around the loop OABC :-

$$\oint \underline{H}.d\underline{l} = 0 \qquad \text{A7}$$

or

$$\int_O^A \underline{H}.d\underline{l} + \int_A^B \underline{H}.d\underline{l} + \int_B^C \underline{H}.d\underline{l} = H_i L \qquad \text{A8}$$

where H_i is assumed constant along OC.

Taking $\sigma(r) = \sigma$ for the end-caps gives:-

$$\int_O^A \underline{H}.d\underline{l} = \int_B^C \underline{H}.d\underline{l} = \frac{Q_e}{4\pi\mu_o\mu t} \qquad \text{A9}$$

Similarly with $\sigma(l) = \sigma_o(1 - 2l/L)$ for the side-walls :-

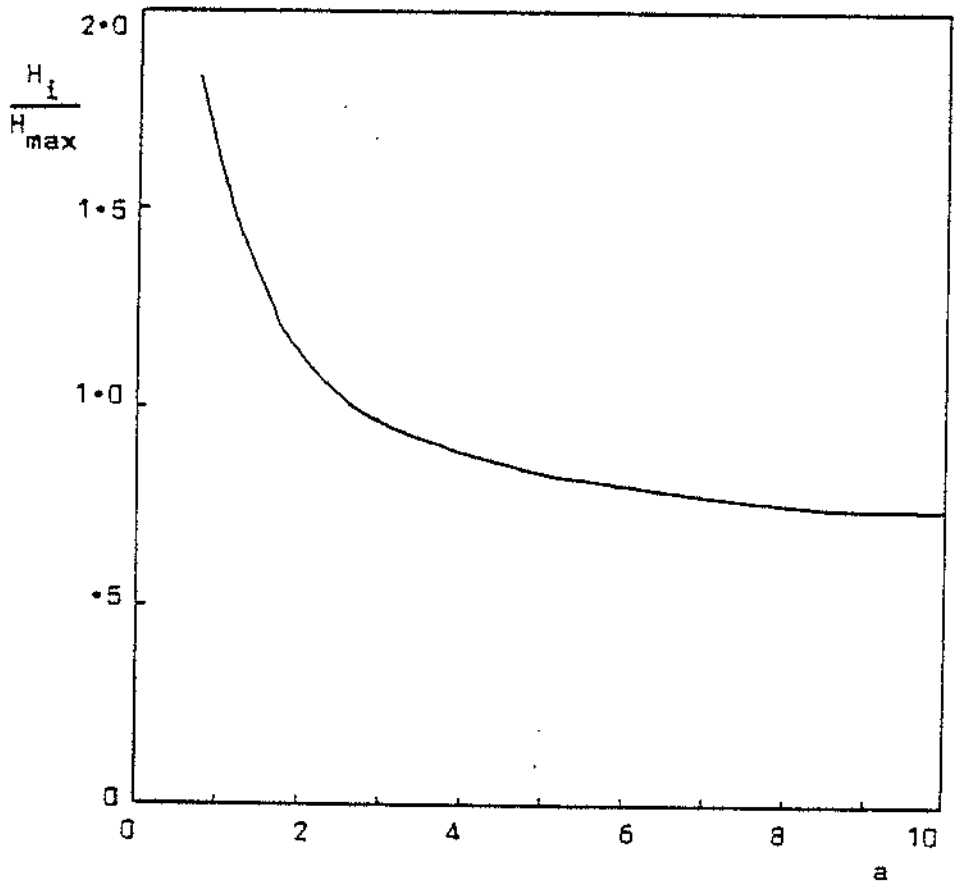

FIG A4 : Variation of H_i/H_{max} with a for a single layer.

$$\int_A^B \underline{H}.d\underline{l} = \frac{Q_e a}{2\pi\mu_o\mu t}(1 + \frac{\alpha a}{3}) \qquad A10$$

Thus:-

$$H_i = \frac{Q_e}{2\pi\mu_o\mu t L}(1 + a + \frac{\alpha a^2}{3}) \qquad A11$$

Combining this with 2•35 and 2•37 gives:-

$$\frac{H_i}{H_{max}} = \frac{(1 + a + \alpha a^2/3)}{a(1 + \alpha a/2)} \qquad A12$$

Using $\alpha = 0{\cdot}85$ this is plotted as a function of a in FIG A4.

(c) Shielded solenoid calculations.

The problem is to calculate the field produced by a coil enclosed by a magnetic shield as shown in FIG 3•11. Solutions will be found both for conventional and superconducting shields.

(i) Conventional shielding.

Adding three extra terms to those used by Hanson and Pipkin (reference (17)) the vector potential can be written[104]:-

$$A_\rho = A_z = 0 \qquad A13$$

$$A_\phi = \sum_{n,k}(A_n I_n'(k\rho) + B_n K_n'(k\rho))\cos(kz + \gamma_k)\sin(n\phi + \delta_n) + \frac{Fz}{\rho} + \frac{G}{\rho} + H\rho$$

Symmetry requires that $A_\phi \neq A_\phi(\phi)$, and hence $n = \delta_n = 0$, and also that $\gamma_k = 0$. The vector potential then becomes:-

$$A_\phi = \sum_k (A_k I_1(k\rho) + B_k K_1(k\rho))\cos(kz) + \frac{F_1 z}{\rho} + \frac{G_1}{\rho} + H_1\rho \qquad \rho > a$$

A14

$$A_\phi = \sum_k C_k I_1(k\rho)\cos(kz) + H_2\rho \qquad \rho < a$$

From these the radial magnetic field component, B_ρ, is:-

$$B_\rho = \sum_k k(A_k I_1(k\rho) + B_k K_1(k\rho))\sin(kz) - \frac{F_1}{\rho} \qquad \rho > a$$

A15

$$B_\rho = \sum_k kC_k I_1(k\rho)\sin(kz) \qquad \rho < a$$

With high permeability material the flux will enter the material normally and hence for $z = \pm h$ $B_\rho = 0$, which implies $k = m\pi/h$ and $F_1 = 0$. Similarly for $\rho = b$ $B_z = 0$, which implies $A_k I_0(kb) = B_k K_0(kb)$ and $H_1 = 0$. This gives:-

$$B_z = \sum_k kA_k \frac{R_0(kb\rho)}{K_0(kb)}\cos(kz) \qquad \rho > a$$

A16

$$B_z = \sum_k kC_k I_0(k\rho)\cos(kz) + 2H_2 \qquad \rho < a$$

where $R_0(kst) = K_0(ks)I_0(kt) - I_0(ks)K_0(kt)$.

Continuity of A_ϕ across $\rho = a$ further gives:-

$$B_z = \sum_k kC_k R_0(kb\rho)I_1(ka)\cos(kz) \qquad \rho > a$$

A17

$$B_z = \sum_k kC_k R_1(kba)I_0(k\rho)\cos(kz) + 2H_2 \qquad \rho < a$$

where $R_1(kst) = K_0(ks)I_1(kt) + I_0(ks)K_1(kt)$.

From A17:-

$$B_z(\rho=a^-) - B_z(\rho=a^+) = \sum_k \frac{1}{a} C_k I_o(kb)\cos(kz) + 2H_2 \qquad \text{A18}$$

Also:-

$$B_z(\rho=a^-) - B_z(\rho=a^+) = \mu_o NI \qquad -c \leq z \leq c$$

$$= 0 \qquad c < |z| < h \qquad \text{A19}$$

where N is the number of turns per unit length and I the current. Solving A18 and A19 for C_k gives:-

$$C_k = \frac{2\mu_o NIa}{kI_o(kb)}\sin(kc) \qquad \text{A20(a)}$$

and $$C_o = 2H_2 = \mu_o NI\frac{c}{h} \qquad \text{A20(b)}$$

Thus finally:- $k = n\pi/h$

$$B_z(\rho,z) = \mu_o NI\left(\frac{c}{h} + \frac{2a}{h}\left(\sum_k R_1(kba)\frac{I_o(k\rho)}{I_o(kb)}\sin(kc)\cos(kz)\right)\right) \qquad \rho < a \qquad \text{A21(a)}$$

which agrees with that quoted by Balling[60], and,

$$B_\rho(\rho,z) = 2\mu_o NI\frac{a}{h}\sum_k R_1(kba)\frac{I_1(k\rho)}{I_o(kb)}\sin(kc)\sin(kz) \qquad \rho < a \qquad \text{A21(b)}$$

(ii) Superconducting shielding.

Starting with the same vector potential, A13, the problem can be solved in exactly the same way except that the boundary

conditions at $z = \pm h$ and $\rho = b$ become:-

$$B_z(\rho, \pm h) = B(b,z) = 0 \qquad \text{A22}$$

The final results are then:-

$$B_z(\rho,z) = -2\mu_o NI\frac{a}{h}\sum_k S_1(kab)\frac{I_o(k\rho)}{I_1(kb)}\text{Sin}(kc)\text{Cos}(kz) \qquad \rho < a$$

A23

$$B_\rho(\rho,z) = -2\mu_o NI\frac{a}{h}\sum_k S_1(kab)\frac{I_1(k\rho)}{I_1(kb)}\text{Sin}(kc)\text{Sin}(kz) \qquad \rho < a$$

where $S_1(kst) = I_1(ks)K_1(kt) - K_1(ks)I_1(kt)$

and $k = (m + \frac{1}{2})/h$.